

Decentralized MIMO Systems with LMMSE Receivers and Imperfect CSI

Zeyan Zhuang, Xin Zhang, Dongfang Xu, Shenghui Song, *Senior Member, IEEE*, and Yonina C. Eldar, *Fellow, IEEE*

Abstract—Centralized baseband processing (CBP) is required to achieve the full potential of massive multiple-input multiple-output (MIMO) systems. However, due to the large number of antennas, CBP suffers from two major issues: 1) Tremendous data interconnection between radio frequency (RF) circuitry and processing fabrics; and 2) high-dimensional computation. To this end, decentralized baseband processing (DBP) has been proposed, where the antennas at the BS are partitioned into clusters connected to separate RF circuits and equipped with separate computing units. Unfortunately, due to the decentralized structure, the optimal fusion scheme and performance analysis for DBP with general spatial correlation between clusters and imperfect channel state information (CSI) are not available in the literature. In this paper, we consider a decentralized MIMO system where all clusters adopt linear minimum mean-square error (LMMSE) receivers with imperfect CSI. Specifically, we first establish the optimal linear fusion scheme which has high computational and data input/output (I/O) costs. To reduce the costs, we further propose two sub-optimal fusion schemes with reduced complexity. For all three schemes, we derive the closed-form expressions for the signal-to-interference-and-noise ratio (SINR) by leveraging random matrix theory (RMT) and demonstrate the conditions under which the sub-optimal schemes are optimal. Furthermore, we determine the optimal regularization parameter for decentralized LMMSE receivers, identify the best antenna partitioning strategy, and prove that the SINR will decrease as the number of clusters increases. Numerical simulations validate the accuracy of the theoretical results.

Index Terms—decentralized baseband processing (DBP), massive multiple-input-multiple-output (MIMO), linear minimum mean-square error (LMMSE), random matrix theory (RMT).

I. INTRODUCTION

Massive multi-input-multi-output (MIMO) technology has been shown very effective in achieving high spectral efficiency, energy efficiency, and link reliability [1]. However, conventional implementations require centralized baseband processing (CBP) where all baseband data are collected and processed by a centralized baseband processing unit (BBU) [2], [3]. Such centralized processing will cause significant challenges when the size of the antenna arrays becomes extremely large. On the one hand, transmitting baseband data from a large number of BS antennas to the BBU will result in very high throughput demands. On the other hand, traditional detection or beamforming algorithms require the inversion of high-dimensional matrices, which causes heightened computational complexity. These challenges make CBP very difficult to implement in practice [4], [5].

To address the bandwidth and computing bottlenecks of CBP, a more efficient architecture called decentralized baseband processing (DBP) was recently proposed [2], [4], [6]–[8]. With DBP, BS antennas are divided into several clusters, each equipped with its own local computing fabric that performs signal processing tasks in a parallel and decentralized manner. Some engaging results have been achieved for both performance analysis and system design of the DBP architecture. In particular, Li *et al.* [4], [6] developed iterative decentralized

detection algorithms to minimize the mean squared error (MSE) of the received symbols. A gradient descent based decentralized algorithm was proposed in [7] to obtain zero-forcing (ZF) equalization for a daisy chain architecture. In [2], [9], the feedforward DBP architecture was proposed to reduce the latency by avoiding the information exchange between clusters required by previous works [10].

With the feedforward structure, the detection results from all clusters and some middle-stage information are transferred to and fused at the central unit (CU). As a result, the fusion algorithm at the CU is very crucial for successful detection. In [2], Jeon *et al.* provided the optimal linear fusion that maximizes the signal-to-interference-and-noise ratio (SINR) in uncorrelated Rayleigh channels with perfect channel state information (CSI). The closed-form deterministic approximations of the SINR for maximum ratio combining (MRC), ZF, and linear minimum mean-square error (LMMSE) receivers were also derived. The design of the fusion coefficients for decentralized MIMO systems resembles that of the collaboration among access points (APs) in cell-free massive MIMO (CF-mMIMO) systems, where distributed APs are deployed and linked to a central processing unit (CPU) [11]. The difference between DBP and CF-mMIMO lies in the spatial correlation between different clusters, which makes the DBP architecture more general. In [12], four levels of minimum mean-square error (MMSE) receiver cooperation for CF-mMIMO systems were proposed with spatially correlated fading and imperfect CSI. However, the fusion scheme and performance analysis for DBP with general spatial correlation and imperfect CSI are not available in the literature.

In this paper, we consider the feedforward decentralized massive MIMO systems with LMMSE receivers because of their near-optimal performance and ease of implementation [10]. Furthermore, we will consider the case with imperfect CSI, due to the difficulty in obtaining perfect CSI in massive MIMO systems [13], [14]. Specifically, we first determine the optimal linear fusion for the concerned system, which requires global CSI and has high complexity. To reduce the cost, we propose two linear fusion schemes with reduced computation and communication workloads. In particular, the first scheme utilizes a moderate amount of intermediate results computed by the clusters, while the second scheme can be implemented by a fully decentralized (FD) architecture [2], where the CU only needs to calculate the weighted sum of the local detection results, without requiring any other intermediate results.

We then evaluate the performance of the proposed linear fusion schemes. Unfortunately, the presence of channel estimation (CE) errors and the decentralized structure make it very challenging to analyze the receive SINR. To this end, we adopt the large random matrix theory (RMT), which has been proven effective in analyzing the fundamental limits of centralized LMMSE receivers [15], [16]. In fact, the SINR analysis for the DBP architecture in [2] also relied on RMT,

but assumed perfect CSI and uncorrelated Rayleigh channel. In this paper, we analyze the decentralized massive MIMO system with more general settings, which takes the analysis in [2], [15], [16] as special cases. Based on the analysis results, we further investigate the impacts of several key system parameters, including the regularization parameter, the antenna partitioning strategy, and the number of clusters.

The main contributions can be summarized as follows:

- 1) For the concerned decentralized massive MIMO systems, we first derive the optimal linear fusion scheme to maximize the SINR and demonstrate that the optimal coefficients also minimize the MSE for estimating the transmit signal.
- 2) Given the optimal fusion scheme requires global CSI and has high complexity, we propose two sub-optimal fusion schemes that only require local CSI and have reduced levels of complexity.
- 3) We derive the deterministic approximations of the SINR for all three fusion schemes by RMT. The analysis results reveal that, without spatial correlation between clusters or CE errors, the first sub-optimal fusion scheme achieves the optimal performance. Moreover, the second sub-optimal fusion scheme can achieve the optimal performance when there is no spatial correlation between clusters.
- 4) To obtain more physical insights, we derive the closed-form expressions for the SINR over independent and identically distributed (i.i.d.) channels. Based on the results, we further determine the optimal regularization parameters and optimal antenna partition strategies that maximize SINR, and evaluate the impact of the number of clusters.
- 5) From the RMT perspective, we derive the deterministic approximations for linear functions of the resolvent for covariance matrices with generally correlated columns, and demonstrate the convergence rates of the means are $\mathcal{O}(N^{-\frac{1}{2}})$. These findings can be applied to the analysis of regularized zero-forcing (RZF) precoding in the downlink MIMO systems [17].

The rest of the paper is organized as follows. In Section II, we introduce the system model and the DBP architecture. In Section III, we prove the optimal linear fusion scheme and propose two linear fusion schemes for decentralized implementation. In Section IV, we derive the deterministic approximations for the SINR of proposed fusion schemes and investigate the results with i.i.d. channels. Numerical results are given in Section V and Section VI concludes the paper.

Notations: Throughout the paper, lowercase and uppercase boldface letters represent vectors and matrices, respectively. \mathbb{C}^N and $\mathbb{C}^{N \times M}$ denote the space of N -dimensional complex vectors and the space of N -by- M complex matrices, respectively. The conjugate transpose and transpose operator are denoted by $(\cdot)^H$ and $(\cdot)^T$, respectively. $[\mathbf{A}]_{i,j}$ and $[\mathbf{a}]_i$ represent the (i,j) -th entry of matrix \mathbf{A} and i -th element of \mathbf{a} , respectively. For integer vectors $\boldsymbol{\tau} = [\tau_1, \dots, \tau_{N_1}]^T$ and $\boldsymbol{\beta} = [\beta_1, \dots, \beta_{N_2}]^T$, we use notations $\mathbf{A}[\boldsymbol{\tau}, \boldsymbol{\beta}]$ and $\mathbf{A}[\boldsymbol{\tau}, :]$ to denote the submatrices of \mathbf{A} with $[\mathbf{A}[\boldsymbol{\tau}, \boldsymbol{\beta}]]_{i,j} = [\mathbf{A}]_{\tau_i, \beta_j}$ and $[\mathbf{A}[\boldsymbol{\tau}, :]]_{i,j} = [\mathbf{A}]_{\tau_i, j}$, respectively. $\|\cdot\|$ denotes the spectral norm of a matrix or the Euclidean norm of a vector. $\text{Tr } \mathbf{A}$ refers to the trace of \mathbf{A} . \mathbf{I}_N represents the identity matrix of size N and $\mathbf{1}_N$ represents

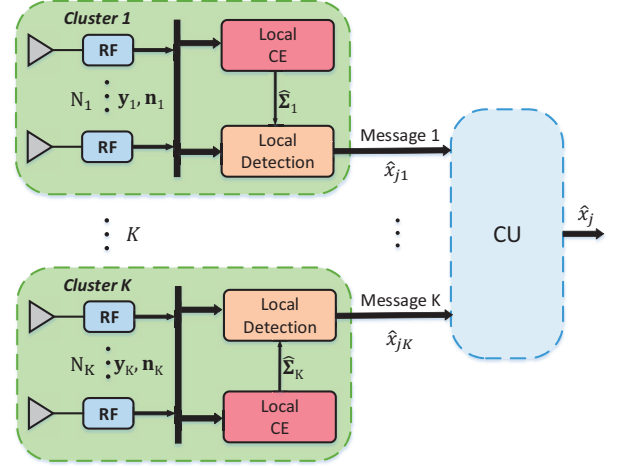


Fig. 1. The feedforward DBP architecture for massive MIMO uplink.

vector with all 1 entries of size N , respectively. The probability measure and the expectation operator are denoted by $\mathbb{P}[\cdot]$ and $\mathbb{E}[\cdot]$, respectively. $\underline{x} = x - \mathbb{E}x$ denotes the centered form of random variable x . $\xrightarrow{a.s.}$ indicates almost sure convergence. The notations $[N]$ and $[N]_0$ represent the set $\{1, 2, \dots, N\}$ and $\{0\} \cup [N]$, respectively. The indicator function is represented by $\mathbb{I}_{\{\cdot\}}$. $\mathcal{O}(\cdot)$ represents the standard Big-O notations. Specifically, we have $f(N) = \mathcal{O}(g(N))$ if and only if there exists a positive real number C and positive integer N_0 such that $|f(N)| \leq Cg(N)$ for all $N \geq N_0$.

II. SYSTEM MODEL

A. Signal Model

Consider an uplink MIMO system where $M + 1$ single-antenna users transmit signals to one BS with N antennas. We denote the transmit signal of all users as $\mathbf{x} = [x_0, \dots, x_M]^T \sim \mathcal{CN}(0, \mathbf{I}_{M+1})$, where x_j represents the signal of user j . The channel between user j and the BS is denoted by $\mathbf{h}_j \in \mathbb{C}^N$. Thus, the received signal at BS is given by

$$\mathbf{y} = \boldsymbol{\Sigma} \mathbf{x} + \mathbf{n}, \quad (1)$$

where $\mathbf{y} \in \mathbb{C}^N$, $\boldsymbol{\Sigma} = [\mathbf{h}_0, \dots, \mathbf{h}_M] \in \mathbb{C}^{N \times (M+1)}$, and $\mathbf{n} \sim \mathcal{CN}(0, \sigma^2 \mathbf{I}_N)$ denotes the additive Gaussian white noise (AWGN) at the BS.

Decentralized Architecture: In this paper, we consider the decentralized architecture [2], [4] as shown in Fig. 1, where the N antennas of the BS are divided into K clusters, connected to one CU. The k -th cluster consists of N_k antennas, and each cluster contains its own RF components and computing fabrics. For simplicity, we partition the received signal $\mathbf{y} = [\mathbf{y}_1^T, \dots, \mathbf{y}_K^T]^T$, the channel matrix $\boldsymbol{\Sigma} = [\boldsymbol{\Sigma}_1^T, \dots, \boldsymbol{\Sigma}_K^T]^T$, the channel vector $\mathbf{h}_j = [\mathbf{h}_{j1}^T, \dots, \mathbf{h}_{jK}^T]^T$, $j \in [M]_0$, and the noise vector $\mathbf{n} = [\mathbf{n}_1^T, \dots, \mathbf{n}_K^T]^T$, such that the received signal at the k -th cluster is given by

$$\mathbf{y}_k = \boldsymbol{\Sigma}_k \mathbf{x} + \mathbf{n}_k, \quad k \in [K], \quad (2)$$

with $\mathbf{y}_k \in \mathbb{C}^{N_k}$, $\boldsymbol{\Sigma}_k \in \mathbb{C}^{N_k \times (M+1)}$, and $\mathbf{n}_k \in \mathbb{C}^{N_k}$. To detect the signal from user j , cluster k independently processes the baseband data to compute the estimate \hat{x}_{jk} . The local estimate \hat{x}_{jk} and a moderate amount of intermediate results are then transferred to the CU. These intermediate results are designed based on the detection scheme and typically include the Gram matrices of the channels [18], [19] or variances of the estimation

errors [2]. The CU will obtain the final estimate \hat{x}_j through linear fusion as

$$\hat{x}_j = \sum_{k=1}^K \alpha_k \hat{x}_{jk}, \quad (3)$$

where α_k represents the fusion coefficient that can be chosen as constant or determined based on the information from clusters. With CBP, the optimal detector is the maximum likelihood detector, which is nonlinear and computationally complex. To reduce the complexity, LMMSE detection is widely used due to its simplicity in implementation and near-optimal performance [10]. Therefore, we consider the case where all clusters adopt LMMSE detection and the detailed design schemes will be discussed in Section III.

B. Channel Model

Due to limited angular spread and insufficient antenna spacing, spatial correlation between BS antennas is inevitable. In this paper, we consider the Rayleigh channel model [20], [21]

$$\mathbf{h}_j = \mathbf{R}_j^{\frac{1}{2}} \mathbf{z}_j, \quad j \in [M]_0, \quad (4)$$

where $\mathbf{R}_j \in \mathbb{C}^{N \times N}$ is a nonnegative definite matrix that models the spatial correlation of the BS antennas with respect to (w.r.t.) user j and $\mathbf{z}_j \sim \mathcal{CN}(0, \mathbf{I}_N)$. Note that this model takes the variance profile model [15], [22] as a special case. With DBP, each cluster k can only know its local spatial correlation matrix, which is a principal submatrix of \mathbf{R}_j . To this end, we denote the index vector

$$\varsigma_k = \left[\sum_{i=1}^{k-1} N_i + 1, \sum_{i=1}^{k-1} N_i + 2, \dots, \sum_{i=1}^k N_i \right]^T, \quad k \in [K], \quad (5)$$

and for a N -by- N matrix \mathbf{R} , we define

$$[\mathbf{R}]_{[k,l]} = \mathbf{R}[\varsigma_k, \varsigma_l]. \quad (6)$$

As a result, the spatial correlation of the k -th cluster is denoted by $[\mathbf{R}_j]_{[k,k]}$.

Decentralized Channel Estimation: To obtain the CSI, user j will transmit its pilot signal that is orthogonal to those of other users. The k -th cluster estimates its local channel vector \mathbf{h}_{jk} based on the observation $\tilde{\mathbf{y}}_{jk} \in \mathbb{C}^{N_k}$, given by [23]

$$\tilde{\mathbf{y}}_{jk} = \mathbf{h}_{jk} + \tilde{\mathbf{n}}_{jk}, \quad j \in [M]_0, k \in [K], \quad (7)$$

where $\tilde{\mathbf{n}}_{jk} \sim \mathcal{CN}(0, \tilde{\sigma}^2 \mathbf{I}_{N_k})$ denotes the AWGN noise. For ease of illustration, we absorb the pilot transmit power and the pilot sequence length into the training SNR $\frac{1}{\tilde{\sigma}^2}$. Moreover, the training SNR is assumed known at each cluster. Under such circumstances, the MMSE estimate $\hat{\mathbf{h}}_{jk}$ of \mathbf{h}_{jk} is given by [24]

$$\hat{\mathbf{h}}_{jk} = [\mathbf{R}_j]_{[k,k]} ([\mathbf{R}_j]_{[k,k]} + \tilde{\sigma}^2 \mathbf{I}_{N_k})^{-1} \tilde{\mathbf{y}}_{jk}. \quad (8)$$

Stacking the channel estimate of all clusters as $\hat{\mathbf{h}}_j = [\hat{\mathbf{h}}_{j0}^T, \dots, \hat{\mathbf{h}}_{jK}^T]^T$, the distribution of the channel vector can be expressed as

$$\begin{aligned} \hat{\mathbf{h}}_j &\sim \mathcal{CN}(\mathbf{0}, \Phi_j), \\ \mathbf{h}_j | \hat{\mathbf{h}}_j &\sim \mathcal{CN}(\mathbf{V}_j \hat{\mathbf{h}}_j, \mathbf{W}_j), \end{aligned} \quad (9)$$

where the second line can be obtained by the linearity property of the posterior mean of Gaussian distributions [25]. Matrices Φ_j , \mathbf{V}_j , and \mathbf{W}_j are defined as

$$\Phi_j = \mathbf{D}_{T,j}(\tilde{\sigma}^2 \mathbf{I}_N + \mathbf{R}_j) \mathbf{D}_{T,j}^T,$$

$$\mathbf{V}_j = \mathbf{T}_j \mathbf{D}_{T,j}^{-1}, \quad \mathbf{W}_j = \tilde{\sigma}^2 \mathbf{T}_j, \quad (10)$$

where $\mathbf{T}_j = \mathbf{R}_j(\tilde{\sigma}^2 \mathbf{I}_N + \mathbf{R}_j)^{-1}$, $\mathbf{D}_{R,j} = \text{diag}([\mathbf{R}_j]_{[k,k]}; k \in [K])$, and $\mathbf{D}_{T,j} = \mathbf{D}_{R,j}(\tilde{\sigma}^2 \mathbf{I}_N + \mathbf{D}_{R,j})^{-1}$. When the spatial correlation between antennas of different clusters is negligible, i.e., $\mathbf{R}_j = \mathbf{D}_{R,j}$ and $\mathbf{V}_j = \mathbf{I}_N$, $\hat{\mathbf{h}}_j$ is the same as that estimated by the centralized MMSE estimator. Therefore, \mathbf{V}_j represents the effect of decentralized CE. For ease of notations, we define $\hat{\mathbf{\Sigma}} = [\hat{\mathbf{h}}_0, \dots, \hat{\mathbf{h}}_M]$, $\hat{\mathbf{\Sigma}}_k = [\hat{\mathbf{h}}_{0k}, \dots, \hat{\mathbf{h}}_{Mk}]$, $\tilde{\mathbf{h}}_j = \mathbf{V}_j \hat{\mathbf{h}}_j$, $\tilde{\mathbf{\Sigma}} = [\tilde{\mathbf{h}}_0, \dots, \tilde{\mathbf{h}}_M]$, and $\mathbf{W} = \sum_{j \in [M]_0} \mathbf{W}_j$.

III. DECENTRALIZED LMMSE RECEIVER AND LINEAR FUSION

In this section, we first introduce the decentralized LMMSE receiver, and derive the optimal linear fusion scheme which requires global CSI and has high complexity. Then, we propose two linear fusion schemes, which only require local CSI and have reduced complexity.

A. Decentralized LMMSE Receiver

Without loss of generality, we consider the detection of x_0 . In particular, the k -th cluster will utilize \mathbf{r}_k to obtain the estimate $\hat{x}_{0k} = \mathbf{r}_k^H \mathbf{y}_k$ that minimizes the local MSE

$$\text{MSE}_k = \mathbb{E}_{\mathbf{x}, \mathbf{n}} |\hat{x}_{0k} - x_0|^2. \quad (11)$$

In the presence of CE errors, the local MSE should be calculated by taking the average over the posterior distribution $\Sigma_k | \hat{\Sigma}_k$ [26], which yields

$$\text{MSE}_k | \hat{\Sigma}_k = \mathbb{E}_{\Sigma_k | \hat{\Sigma}_k, \mathbf{x}, \mathbf{n}} |\hat{x}_{0k} - x_0|^2. \quad (12)$$

Hence, the optimal \mathbf{r}_k to minimize $\text{MSE}_k | \hat{\Sigma}_k$ is given by

$$\mathbf{r}_k^{\text{mmse}} = \left(\hat{\Sigma}_k \hat{\Sigma}_k^H + N_k \mathbf{Z}_k + N_k \rho_k \mathbf{I}_{N_k} \right)^{-1} \hat{\mathbf{h}}_{0k}, \quad (13)$$

where $\rho_k = \frac{\sigma^2}{N_k}$ and

$$\mathbf{Z}_k = \frac{\tilde{\sigma}^2}{N_k} \sum_{j=0}^M [\mathbf{R}_j]_{[k,k]} ([\mathbf{R}_j]_{[k,k]} + \tilde{\sigma}^2 \mathbf{I}_{N_k})^{-1}. \quad (14)$$

Note that the above ρ_k and \mathbf{Z}_k minimize the local MSE, but may not be optimal after fusion. As a result, we treat ρ_k and \mathbf{Z}_k as design parameters that can be optimized and refer to ρ_k as the regularization parameter in the subsequent.

With the linear fusion in (3), the achievable rate of user 0 can be bounded by a standard lower bound $R_0 = \log(1 + \gamma_0)$ based on the worst-case uncorrelated additive noise [27]. Here, γ_0 is the associated SINR given by

$$\gamma_0 = \frac{\left| \mathbb{E}_{\mathbf{h}_0 | \hat{\mathbf{h}}_0} [\mathbf{r}_\alpha^H \mathbf{h}_0] \right|^2}{\mathbb{E}_{\Sigma | \hat{\Sigma}, \mathbf{x}, \mathbf{n}} \left| \mathbf{r}_\alpha^H [\Sigma \mathbf{x} - \tilde{\mathbf{h}}_0 x_0 + \mathbf{n}] \right|^2}, \quad (15)$$

with $\mathbf{r}_\alpha = [\alpha_1^* \cdot (\mathbf{r}_1^{\text{mmse}})^T, \dots, \alpha_K^* \cdot (\mathbf{r}_K^{\text{mmse}})^T]^T \in \mathbb{C}^N$. Next, we determine the optimal fusion coefficients $\alpha_1, \dots, \alpha_K$ that can maximize the SINR γ_0 in (15) [2].

B. Linear Fusion with Optimal Coefficients

The following proposition provides the optimal linear fusion scheme that maximizes the SINR and demonstrates that it also minimizes the MSE for estimating the transmit signal.

Proposition 1. The optimal coefficients $\alpha^T = [\alpha_1, \dots, \alpha_K]^T$ for maximizing (15) are given by

$$\alpha^{\text{opt}} = c \tilde{\mathbf{h}}_0^H \mathbf{D}_r \left(\mathbf{D}_r^H (\tilde{\Sigma} \tilde{\Sigma}^H + \mathbf{W} + \sigma^2 \mathbf{I}_N) \mathbf{D}_r \right)^{-1}, \quad (16)$$

where $c \in \mathbb{C} \setminus \{0\}$ and $\mathbf{D}_r = \text{diag}(\mathbf{r}_k^{\text{mmse}}; k \in [K])$. When $c = 1$, α^{opt} is also the optimal solution for the following MMSE problem

$$\underset{\alpha}{\text{minimize}} \quad \text{MSE}|_{\hat{\Sigma}} = \mathbb{E}_{\Sigma|\hat{\Sigma}, \mathbf{x}, \mathbf{n}} \left| \sum_{k=1}^K \alpha_k \hat{x}_{0k} - x_0 \right|^2. \quad (17)$$

Proof: The proof of Proposition 1 is given in Appendix A. \square

Remark 1. The optimality of α^{opt} in Proposition 1 holds for any linear receivers, e.g., MRC, and LMMSE is a special case.

Remark 2. It can be verified that when $c = 1$ and $\alpha = \alpha^{\text{opt}}$, we have $\text{MSE}|_{\hat{\Sigma}} = (1 + \gamma_0)^{-1} = \frac{d \log(1 + \gamma_0)}{d \gamma_0}$, which reveals the connection between mutual information and MSE. This relation can be generalized to the case with non-Gaussian signal input [28].

Remark 3. Proposition 1 shows that the fusion coefficients that maximize the SINR are actually a scaled version of the parameters that minimize MSE.

We will refer to the fusion scheme in Proposition 1 as linear fusion with optimal coefficients (LFOC) in the following. Note that, due to the presence of spatial correlation between different clusters, one cluster cannot determine the off-diagonal elements of $\mathbf{R}_j - \mathbf{D}_{R,j}$ and the channel $\tilde{\Sigma}$ in the feedforward architecture. As a result, to obtain α^{opt} , the CU needs to know the global CSI, which leads to high I/O and computational cost. To reduce the complexity, we proposed two linear fusion schemes in the following.

C. Linear Fusion with Suboptimal Coefficients

Based on (16), we can design the suboptimal fusion parameter as

$$\alpha^{\text{s-opt}} = \hat{\mathbf{h}}_0^H \mathbf{D}_r \left(\mathbf{D}_r^H (\hat{\Sigma} \hat{\Sigma}^H + \mathbf{D}_W + \sigma^2 \mathbf{I}_N) \mathbf{D}_r \right)^{-1}, \quad (18)$$

where $\mathbf{D}_W = \tilde{\sigma}^2 \sum_{j \in [M]_0} \mathbf{D}_{T,j}$. In particular, the suboptimal solution first replaces Σ in (16) with the estimated channel $\hat{\Sigma}$, and then adopts a block diagonal version of \mathbf{W} . These terms are all computed based on the local CSI and spatial correlations. In fact, we can write

$$[\hat{\mathbf{M}}]_{k,l} = (\mathbf{r}_k^{\text{mmse}})^H \hat{\Sigma}_k \hat{\Sigma}_l^H \mathbf{r}_l^{\text{mmse}} + \mathbb{I}_{\{k=l\}} (\mathbf{r}_k^{\text{mmse}})^H [\mathbf{D}_W + \sigma^2 \mathbf{I}_N]_{[k,k]} \mathbf{r}_k^{\text{mmse}}, \quad (19)$$

$$[\hat{\mathbf{m}}]_k = (\mathbf{r}_k^{\text{mmse}})^H \hat{\mathbf{h}}_{0k}, \quad (20)$$

where $\hat{\mathbf{M}} = \mathbf{D}_r^H (\hat{\Sigma} \hat{\Sigma}^H + \mathbf{D}_W + \sigma^2 \mathbf{I}_N) \mathbf{D}_r$ and $\hat{\mathbf{m}} = \mathbf{D}_r^H \hat{\mathbf{h}}_0$. Therefore, to obtain $\alpha^{\text{s-opt}}$, cluster k needs to compute and transfer the intermediate parameter set

$$\mathcal{P}_k = \{ (\mathbf{r}_k^{\text{mmse}})^H \hat{\mathbf{h}}_{0k}, (\mathbf{r}_k^{\text{mmse}})^H \hat{\Sigma}_k, (\mathbf{r}_k^{\text{mmse}})^H [\mathbf{D}_W + \sigma^2 \mathbf{I}_N]_{[k,k]} \mathbf{r}_k^{\text{mmse}} \} \quad (21)$$

to the CU. Then the CU will use $\mathcal{P}_1, \dots, \mathcal{P}_K$ to determine $\hat{\mathbf{M}}$ and $\hat{\mathbf{m}}$ by (19) and (20), respectively, and compute $\alpha^{\text{s-opt}} = \hat{\mathbf{m}}^H \hat{\mathbf{M}}^{-1}$. Finally, based on (3), \hat{x}_0 could be obtained. We will refer to this scheme as linear fusion with suboptimal coefficients

(LFSC) in the following. Note that the computation and I/O complexity of LFSC is manageable since each parameter in \mathcal{P}_k is a vector or a scalar, and the detailed computational complexity is given in Table I. It can be observed the overall complexity of LFSC is significantly reduced compared to CBP.

D. Linear Fusion with Constant Coefficients

Although LFSC has reduced complexity, it still requires to compute and transmit additional information to the CU. When the number of clusters is very large, the computational complexity, memory requirements, and I/O cost may be very high. To further reduce the complexity, we provide a simple linear fusion scheme with constant coefficients α_k . For example, we can take

$$\alpha_k = \frac{1}{K}, \quad k \in [K], \quad (22)$$

or more heuristically

$$\alpha_k = \frac{N_k}{N}, \quad k \in [K]. \quad (23)$$

We will refer to this scheme as linear fusion with constant coefficients (LFCC) in the following. The complexity of LFCC is also given in Table I which is much lower than that of LFSC. Note that LFCC can be implemented by the FD feedforward architecture [2], where the CU only needs to take the weighted sum of local detection results and does not require any additional intermediate results or processing.

IV. ASYMPTOTIC SINR ANALYSIS

The expression for the SINR γ_0 in (37) contains the correlated terms between the channels $\hat{\Sigma}$ and $\tilde{\Sigma}$, making it very difficult to analyze. In this section, we will investigate the asymptotic behaviors of γ_0 . Specifically, we will show that as the number of antennas and users tend to infinity at the same rate, γ_0 will converge almost surely, and then derive the deterministic approximations for the SINR of the fusion schemes proposed in Section III. To achieve this, we require the following large-scale system assumptions.

Assumption A.1. For a given number of clusters K , we assume $0 < \liminf_N \frac{N_k}{M} \leq \limsup_N \frac{N_k}{M} < +\infty$ for each $k \in [K]$.

Assumption A.2. Assume

$$\limsup_N \sup_{j \in [M]_0} \lambda_M(\mathbf{R}_j) < +\infty, \quad (24a)$$

$$\liminf_N \inf_{j \in [M]_0} \lambda_m(\mathbf{R}_j) > 0, \quad (24b)$$

where $\lambda_M(\mathbf{R}_j)$ and $\lambda_m(\mathbf{R}_j)$ denote the largest and smallest eigenvalue of \mathbf{R}_j , respectively.

Assumption A.3. Assume $\rho_k > 0$ and \mathbf{Z}_k is Hermitian non-negative such that $\limsup_N \sup_{k \in [K]} \|\mathbf{Z}_k\| < +\infty$ for each $k \in [K]$.

A.1 implies that the number of antennas of the k -th cluster N_k and the number of users M approach infinity at the same rate [2]. For simplicity, we define $c_k = \frac{N_k}{M}$ and use $N \xrightarrow{c_1, \dots, c_K} +\infty$ to represent this asymptotic regime. According to interlacing inequalities [29], **A.2** ensures the eigenvalues of the local spatial correlation matrices $[\mathbf{R}_j]_{[k,k]}$ are bounded away from 0, which makes \mathbf{V}_j legal. **A.3** implies that the spectral norm of \mathbf{Z}_k does

TABLE I
COMPARISON FOR THE COMPLEXITY OF DIFFERENT DETECTION METHODS

Detection Algorithm	I/O Throughput of Cluster k	Computational Complexity of Cluster k	Computational Complexity of the CU
Centralized LMMSE	-	-	$\mathcal{O}(N^2M + N^3 + N^2 + N)$
Local LMMSE & LFSC	$\mathcal{O}(M)$	$\mathcal{O}(N_k^2M + N_k^3 + N_kM + N_k^2 + N_k)$	$\mathcal{O}(K^2M + K^3 + K^2 + K)$
Local LMMSE & LFCC	$\mathcal{O}(1)$	$\mathcal{O}(N_k^2M + N_k^3 + N_k^2 + N_k)$	$\mathcal{O}(K)$

not diverge to infinity. If A.1 and A.2 hold, (14) satisfies this assumption.

Let γ^{lloc} , γ^{lfsc} , and γ^{lfcc} denote the SINR with LFOC, LFSC, and LFCC schemes, respectively. The following theorem provides the deterministic approximations for γ^{lloc} , γ^{lfsc} , and γ^{lfcc} , respectively.

Theorem 1. When Assumptions A.1-A.3 hold, the deterministic approximations for γ^{lloc} , γ^{lfsc} , and γ^{lfcc} are given by

$$\gamma^{\text{lloc}} \xrightarrow[N \xrightarrow{c_1, \dots, c_K} + \infty]{a.s.} \bar{\gamma}^{\text{lloc}} = \mathbf{v}^H \mathbf{\Delta}^{-1} \mathbf{v}, \quad (25a)$$

$$\gamma^{\text{lfsc}} \xrightarrow[N \xrightarrow{c_1, \dots, c_K} + \infty]{a.s.} \bar{\gamma}^{\text{lfsc}} = \frac{(\mathbf{v}^H \mathbf{\Delta}_I^{-1} \mathbf{v})^2}{\mathbf{v}^H \mathbf{\Delta}_I^{-1} \mathbf{\Delta} \mathbf{\Delta}_I^{-1} \mathbf{v}}, \quad (25b)$$

$$\gamma^{\text{lfcc}} \xrightarrow[N \xrightarrow{c_1, \dots, c_K} + \infty]{a.s.} \bar{\gamma}^{\text{lfcc}} = \frac{|\alpha \mathbf{J} \mathbf{v}|^2}{\alpha \mathbf{J} \mathbf{\Delta} \mathbf{J} \alpha^H}, \quad (25c)$$

with

$$[\mathbf{v}]_k = \frac{\bar{\Gamma}_k([\Phi_0]_{[k,k]})}{N_k}, \quad (26a)$$

$$\mathbf{J} = [\mathbf{I}_K + \text{diag}(\mathbf{v})]^{-1}, \quad (26b)$$

$$[\mathbf{\Delta}]_{k,l} = \frac{\bar{\Upsilon}_{kl}([\Phi_0]_{[l,k]}, [\mathbf{W} + \sigma^2 \mathbf{I}_N]_{[k,l]})}{N_k N_l} + \frac{\bar{\Pi}_{B,kl}([\Phi_0]_{[l,k]})}{\sqrt{N_k N_l}}, \quad (26c)$$

$$[\mathbf{\Delta}_I]_{k,l} = \frac{\bar{\Upsilon}_{kl}([\Phi_0]_{[l,k]}, [\mathbf{D}_W + \sigma^2 \mathbf{I}_N]_{[k,l]})}{N_k N_l} + \frac{\bar{\Pi}_{kl}([\Phi_0]_{[l,k]})}{\sqrt{N_k N_l}}, \quad (26d)$$

where functions $\bar{\Gamma}_k$, $\bar{\Upsilon}_{kl}$, $\bar{\Pi}_{B,kl}$, and $\bar{\Pi}_{kl}$ can be obtained from Lemma 3 in Appendix C by setting $z_i = -\rho_i$, $\mathbf{S}_i = \mathbf{Z}_i$, $\mathbf{A}_j = \Phi_j^{\frac{1}{2}}$, and $\mathbf{B}_j = \mathbf{V}_j \Phi_j^{\frac{1}{2}}$ for each $i \in [K]$ and $j \in [M]$.

Proof: The proof of Theorem 1 is given in Appendix B. \square

Remark 4. When $K = 1$, which means there is only one cluster, $\bar{\gamma}^{\text{lloc}}$, $\bar{\gamma}^{\text{lfsc}}$, and $\bar{\gamma}^{\text{lfcc}}$ degenerate to the results with centralized LMMSE [15], [16].

Remark 5. Under certain conditions, the performance of LFSC approaches that of LFOC. In particular, when $\mathbf{\Delta}_I = \mathbf{\Delta}$, we have $\bar{\gamma}^{\text{lloc}} = \bar{\gamma}^{\text{lfsc}}$. The above condition can be achieved, when the spatial correlations between clusters are negligible, i.e., $\mathbf{R}_j = \mathbf{D}_{R,j}$ for each $j \in [M]_0$ or the CSI is perfect, i.e., $\tilde{\sigma}^2 = 0$. The equivalence can also be observed from the fact that under the conditions $\tilde{\sigma}^2 \mathbf{R}_j = \tilde{\sigma}^2 \mathbf{D}_{R,j}$ for each $j \in [M]_0$, the LFSC scheme has the same fusion parameters as LFOC, i.e. $\alpha^{\text{s-opt}} = \alpha^{\text{opt}}$.

Remark 6. When there is no spatial correlation between clusters, the matrix $\mathbf{\Delta}$ becomes diagonal. Under such circumstances, it can be verified that when $\alpha = C \left[\frac{(1+[\mathbf{v}]_1)[\mathbf{v}]_1}{[\mathbf{\Delta}]_{1,1}}, \dots, \frac{(1+[\mathbf{v}]_K)[\mathbf{v}]_K}{[\mathbf{\Delta}]_{K,K}} \right]$ with $C \neq 0$ being an arbitrary

constant, we have

$$\bar{\gamma}^{\text{lloc}} = \bar{\gamma}^{\text{lfsc}} = \bar{\gamma}^{\text{lfcc}} = \sum_{k=1}^K \frac{[\mathbf{v}]_k^2}{[\mathbf{\Delta}]_{k,k}}, \quad (27)$$

which is equal to the sum of the SINRs from all clusters. This is consistent with the conclusion of [2, Theorem 6], which assumes uncorrelated Rayleigh channels and perfect CSI. In addition, $[\mathbf{v}]_k$ and $[\mathbf{\Delta}]_{k,k}$ are only related to the local spatial correlation, which varies slowly in time. As a result, the fusion coefficients for LFCC can be set as $\alpha_k = \frac{(1+[\mathbf{v}]_k)[\mathbf{v}]_k}{[\mathbf{\Delta}]_{k,k}}$ to achieve the asymptotically optimal performance.

A. Special Case Study: I.I.D. Channels

In this section, we will consider the simplified channel model with $\mathbf{R}_j = \mathbf{I}_N$ to get some physical insights. The parameter \mathbf{Z}_k is set as (14), i.e., $\mathbf{Z}_k = \frac{(M+1)\tilde{\sigma}^2}{N_k(\tilde{\sigma}^2+1)} \mathbf{I}_{N_k}$.

1) *SINR Approximation:* With i.i.d. channels, the SINR in Theorem 1 can be given in a closed-form.

Corollary 1. Given assumptions A.1-A.3 and the i.i.d. channels, $\bar{\gamma}^{\text{lloc}}$, $\bar{\gamma}^{\text{lfsc}}$ and $\bar{\gamma}^{\text{lfcc}}$ can be given by

$$\bar{\gamma}^{\text{lloc}} = \bar{\gamma}^{\text{lfsc}} = \sum_{k=1}^K \frac{\delta_k}{\varpi_k}, \quad (28a)$$

$$\bar{\gamma}^{\text{lfcc}} = \frac{\left| \sum_{k=1}^K \alpha_k \frac{\delta_k}{1+\delta_k} \right|^2}{\sum_{k=1}^K \frac{|\alpha_k|^2 \delta_k}{(1+\delta_k)^2} \varpi_k}, \quad (28b)$$

where

$$\varpi_k = 1 + \left(\frac{\sigma^2}{M c_k} - \rho_k \right) \frac{(\tilde{\sigma}^2 + 1) \delta_k}{1 - \frac{\delta_k^2}{c_k (1 + \delta_k)^2}} \quad (29)$$

and δ_k is given by

$$\delta_k = \frac{1 - \frac{1}{c_k} - A_k + \sqrt{\left(A_k + \frac{1}{c_k} - 1 \right)^2 + 4A_k}}{2A_k} \quad (30)$$

with $A_k = \rho_k(\tilde{\sigma}^2 + 1) + \frac{M+1}{M c_k} \tilde{\sigma}^2$.

Proof: The proof can be obtained by setting $\mathbf{R}_j = \mathbf{I}_N$ and $\mathbf{Z}_k = \frac{(M+1)\tilde{\sigma}^2}{N_k(\tilde{\sigma}^2+1)}$ in Theorem 1 and is omitted here. \square

Denote $\boldsymbol{\rho}_K = [\rho_1, \dots, \rho_K]^T$ and $\mathbf{c}_K = [c_1, \dots, c_K]^T$. We next investigate the impact of parameters $\boldsymbol{\rho}_K$, \mathbf{c}_K , and the number of clusters K on the SINR $\bar{\gamma}^{\text{lloc}} = \bar{\gamma}_K^{\text{lloc}}(\boldsymbol{\rho}_K, \mathbf{c}_K)$ where we keep N and M fixed.

2) *Regularization Parameter:* The following corollary gives the optimal parameter $\boldsymbol{\rho}_K$.

Corollary 2. Assume the same conditions as Corollary 1. For any $\boldsymbol{\rho}_K > 0$, $\mathbf{c}_K \geq 0$, we have

$$\bar{\gamma}_K^{\text{lloc}}(\boldsymbol{\rho}_K, \mathbf{c}_K) \leq \bar{\gamma}_K^{\text{lloc}}(\boldsymbol{\rho}_K^{\text{opt}}, \mathbf{c}_K), \quad (31)$$

where $\boldsymbol{\rho}_K^{\text{opt}} = \left[\frac{\sigma^2}{M c_1}, \dots, \frac{\sigma^2}{M c_K} \right]^T$.

Proof: The proof of Corollary 2 is given in Appendix E. \square

Remark 7. We can observe that the optimal parameter ρ_K^{opt} that maximizes the SINR is identical to that achieving the minimal local MSE as derived in Section III-A. This can be intuitively obtained from (28a) where the SINR $\bar{\gamma}^{\text{lfoe}}$ is the sum of the SINRs of all clusters.

3) *Antenna Partitioning Strategy:* The following corollary shows the impact of the parameter \mathbf{c}_K .

Corollary 3. Assume the same conditions as Corollary 1 and denote $\rho_K = [\frac{a}{c_1}, \dots, \frac{a}{c_K}]^T$. For any $\mathbf{c}_K \geq 0$ and $\frac{\sigma^2}{M} \leq a$, we have

$$\bar{\gamma}_K^{\text{lfoe}}(\rho_K, \mathbf{c}_K) \leq \bar{\gamma}_K^{\text{lfoe}}(\rho_K, \mathbf{c}_{K,M}), \quad (32)$$

and for any $\mathbf{c}_K \geq 0$ and $\frac{\sigma^2}{M} \leq a \leq \frac{2\sigma^2}{M} + \frac{(M+1)\bar{\sigma}^2}{M(\bar{\sigma}^2+1)}$, we have

$$\bar{\gamma}_K^{\text{lfoe}}(\rho_K, \mathbf{c}_{K,m}) \leq \bar{\gamma}_K^{\text{lfoe}}(\rho_K, \mathbf{c}_K), \quad (33)$$

where $\mathbf{c}_{K,m} = [\bar{c}, \dots, \bar{c}]^T$, $\mathbf{c}_{K,M} = [K\bar{c}, 0, \dots, 0]^T$, and $\bar{c} = \frac{1}{K} \sum_{k=1}^K c_k$.

Proof: The proof of Corollary 3 is given in Appendix F. \square

Remark 8. Inequalities (32) and (33) imply that when the regularization parameter ρ_K is within a certain range, i.e., $\frac{\sigma^2}{M} \leq a$, the system achieves the maximum SINR when the receive antennas are concentrated in one cluster, i.e., the centralized scheme. On the other side, when the antennas are equally partitioned, the system achieves the lowest SINR. This finding aligns with the conclusions in [2, Lemma 7, Lemma 8]. Note that [2] considers a given parameter ρ_K with perfect CSI, but Corollary 3 provides the range for ρ_K with imperfect CSI.

Remark 9. It can be observed that the optimal regularization parameter ρ_K^{opt} in Corollary 2 is within the range such that (32) and (33) hold.

4) *Number of Clusters:* Corollary 3 compares different antenna partitioning strategies with a fixed number of clusters K . Another interesting question to investigate is how the number of clusters K affects the SINR. The following corollary demonstrates this impact.

Corollary 4. Assume the same conditions as Corollary 1 and denote $\rho_K = [\frac{a}{c_1}, \dots, \frac{a}{c_K}]^T$. For any $\frac{\sigma^2}{M} \leq a$, we have

$$\bar{\gamma}_K^{\text{lfoe}}(\rho_K, \mathbf{c}_{K,m}) \geq \bar{\gamma}_{K+1}^{\text{lfoe}}(\rho_{K+1}, \mathbf{c}_{K+1,m}). \quad (34)$$

Proof: The proof of Corollary 4 is given in Appendix G. \square

Remark 10. Since the total number of receive antennas N is fixed, Corollary 4 indicates that as the number of clusters increases, the SINR will monotonically decrease.

Remark 11. It can be verified from the proof of Corollary 4 that

$$\bar{\gamma}_K^{\text{lfoe}}(\rho_K, \mathbf{c}_{K,m}) \geq \frac{N}{(\sigma^2 + M)(\bar{\sigma}^2 + 1) + \bar{\sigma}^2}, \quad (35)$$

and the equality holds when $K \rightarrow +\infty$, which is not achievable since $K \leq N$. From Corollary 3, we know that the equal antenna partitioning strategy has the worst performance. Therefore, for decentralized LMMSE receivers, the SINR is strictly lower bounded by the right hand side (RHS) of (35). When the numbers of antennas and users are large, this lower bound is approximately $\frac{N}{M}$.

V. NUMERICAL RESULTS

In this section, we will verify the accuracy of the theoretical results in Sections IV. We will also demonstrate the impact of several key system parameters over i.i.d. channels, including the regularization parameter, antenna partitioning strategy, and the number of clusters. For simplicity, we use the notation $\mathcal{N}_K = (N_1, \dots, N_K)$ to denote the antenna partitioning strategy. The Monte Carlo (MC) simulation results were obtained from 5000 realizations and are illustrated by markers in all figures.

A. Correlated Channels

We consider a uniform linear array of antennas at the BS. The (m, n) -th entry of the spatial correlation matrix at BS is modeled as [30], [31]

$$[\mathbf{C}(\eta, \delta, d_s)]_{m,n} = \int_{-180}^{180} \frac{1}{\sqrt{2\pi}\delta^2} e^{2\pi j d_s (m-n) \sin(\frac{\pi\phi}{180}) - \frac{(\phi-\eta)^2}{2\delta^2}} d\phi. \quad (36)$$

Here, d_s and ϕ denote the receive antenna spacing and angular spread, respectively, η represents the mean angle, and δ denotes the root-mean-square angle spread. In the simulation, we set $\mathbf{R}_j = \mathbf{C}(\eta_j, \delta_j, 1)$ with $\eta_j = (\frac{j}{180M})^\circ$ and $\delta_j = 10^\circ + (\frac{j}{M10})^\circ$. The parameter ρ_k is set as $\rho_k = \frac{\sigma^2}{N_k}$ and \mathbf{Z}_k is set according to (14) for each $k \in [K]$.

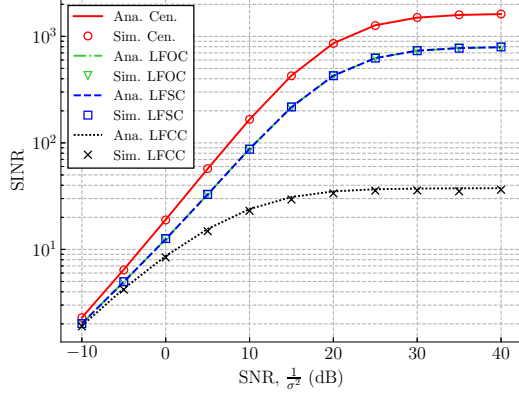
Approximation of SINR: Fig. 2 illustrates the SINR with different linear fusion schemes. The system dimensions are set as $N = 32$, $M = 12$, $K = 2$, and $\mathcal{N}_2 = (10, 22)$. The red line and the black dotted line represent the results of centralized LMMSE and LFCC with $\alpha = [0.5, 0.5]^T$, respectively. By comparing the results with MC simulations, we can observe that the approximation results in Theorem 1 are accurate. By comparing the results of LFSC and LFOC, it can be observed that LFSC is highly efficient. Furthermore, Fig. 2 shows that when the antenna partition is unbalanced, using LFCC will lead to performance degradation.

Impact of Fusion Coefficients: Fig. 3 shows the impact of the fusion coefficients with different antenna partitioning strategies. The system dimensions are set as $N = 40$, $M = 15$, and $K = 2$. The signal and training SNR are both set as 30 dB. It can be observed that when antennas are uniformly allocated to different clusters, i.e., $\mathcal{N}_2 = (20, 20)$, SINR is not sensitive to the value of α , but the maximum SINR is lower than that with unbalanced antenna partitioning. This observation for correlated channels is consistent with the conclusion for i.i.d. channels in Corollary 3. Moreover, as the number of antennas in a cluster increases, the corresponding linear fusion weights should also increase.

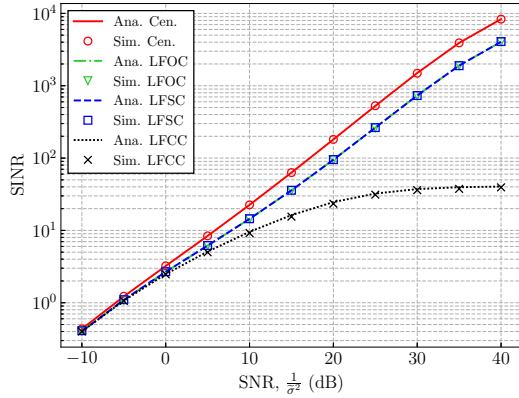
B. I.I.D. Channels

In the experiment, the training and signal SNR are both 30 dB, and the parameter \mathbf{Z}_k is set according to (14) for each $k \in [K]$.

Optimal Regularization Parameter: Fig. 4 depicts the impact of ρ_K on the SINR with i.i.d. channels. The system dimensions are set as $N = 72$ and $M = 40$. The parameter ρ_K is of the form $\rho_K = [\frac{\rho}{N_1}, \dots, \frac{\rho}{N_K}]^T$. It can be observed that SINR is not sensitive to ρ . Significant performance loss is only observed when ρ is very large. Furthermore, according to



(a) SINR versus signal SNR $\frac{1}{\sigma^2}$ with training SNR $\frac{1}{\sigma^2} = -30$ dB.



(b) SINR versus training SNR $\frac{1}{\sigma^2}$ with signal SNR $\frac{1}{\sigma^2} = -30$ dB.

Fig. 2. SINR with different linear fusion schemes.

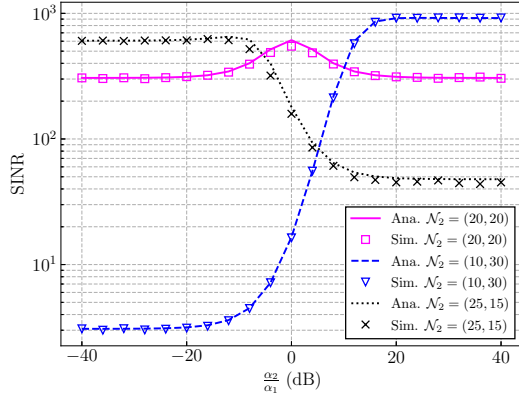


Fig. 3. SINR versus the ratio of fusion coefficients $\frac{\alpha_2}{\alpha_1}$.

Corollary 2, the theoretical optimal parameter ρ_K^{opt} should be $\rho_K^{\text{opt}} = (-30\text{dB}) \cdot [\frac{1}{N_1}, \dots, \frac{1}{N_1}]^T$. The optimal value $\rho^{\text{opt}} = -30$ dB shown in the figure obtained by the exhausted search validates the accuracy of Corollary 2.

Impact of Antenna Partitioning Strategy: In Fig. 5, we plot the SINR for different antenna partitioning strategies with different numbers of users. The parameters are set as $N = 120$, $K = 2$, and $\rho_k = \frac{\sigma^2}{N_k}$. It is observed that when clusters are of equal size, the SINR is the lowest, which agrees with Corollary 3. Furthermore, as the number of users increases,

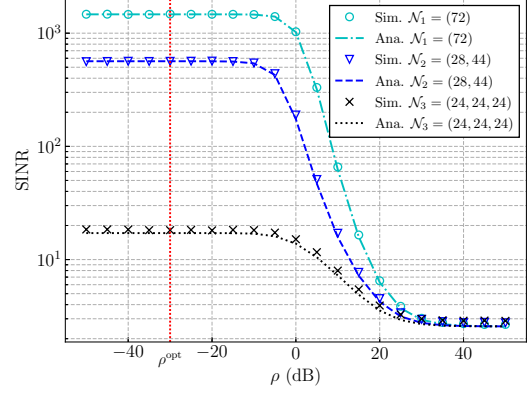


Fig. 4. SINR versus the regularization parameter ρ .

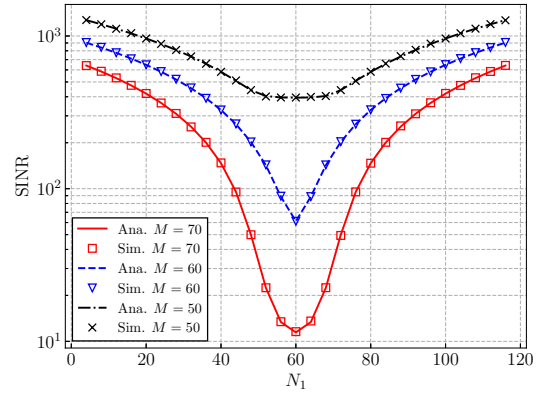


Fig. 5. SINR versus the number of antennas allocated to the first cluster N_1 . the performance degradation with uniform antenna partitioning becomes more obvious.

Impact of Number of Clusters: In Fig. 6, we plot the SINR for different numbers of clusters K where antennas are almost equally allocated with $N_K = (\lfloor \frac{N}{K} \rfloor, \lfloor \frac{N}{K} \rfloor, \dots, N - (K - 1)\lfloor \frac{N}{K} \rfloor)$. The parameters are set as $M = 40$ and $\rho_k = \frac{\sigma^2}{N_k}$. It can be observed that as the number of clusters increases, the SINR decreases monotonically and is lower bounded by (35), which is shown by the dashed lines. This validates Corollary 4.

VI. CONCLUSION

In this paper, we considered the decentralized MIMO systems with LMMSE receivers and imperfect CSI. It was shown that with DBP, the linear fusion coefficients that maximize the receive SINR also minimize the MSE for estimating the transmit signal. To reduce the complexity, we further proposed two linear fusion schemes and derived the deterministic approximations of the SINR with imperfect CSI and general spatial correlations. Based on the results, we investigated the optimal LMMSE regularization parameters, optimal antenna partitioning strategies, and the impact of the number of clusters. It was shown that with i.i.d. channels, the SINR is minimized when the clusters are of equal size. Conversely, the optimal performance is achieved when antennas are mostly unbalanced distributed, i.e., all antennas are allocated to a single cluster. We also proved that as the number of clusters increases, the SINR monotonically decreases.

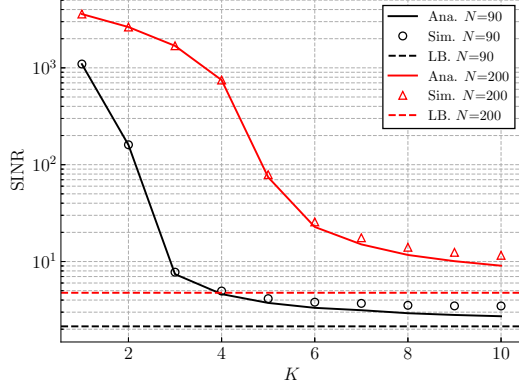


Fig. 6. SINR versus K .

From the perspective of RMT, we investigated the asymptotic convergence properties of the resolvent for the covariance matrix with generally correlated columns and its related functions. These results can be utilized for the second-order SINR analysis, e.g., the outage probability, and also be applied to downlink scenarios, e.g., the analysis of RZF.

APPENDIX A PROOF OF PROPOSITION 1

Denote $\tilde{\mathbf{H}} = [\tilde{\mathbf{h}}_1, \dots, \tilde{\mathbf{h}}_M]$ and $\hat{\mathbf{H}}_k = [\hat{\mathbf{h}}_{1k}, \dots, \hat{\mathbf{h}}_{Mk}]$. Straight-forward computations of (15) yield to

$$\gamma_0 = \frac{\alpha \mathbf{m} \mathbf{m}^H \alpha^H}{\alpha \mathbf{M} \alpha^H}, \quad (37)$$

where $\mathbf{M} = \mathbf{D}_r^H (\tilde{\mathbf{H}} \tilde{\mathbf{H}}^H + \mathbf{W} + \sigma^2 \mathbf{I}_N) \mathbf{D}_r$ and $\mathbf{m} = \mathbf{D}_r^H \tilde{\mathbf{h}}_0$. One can validate that \mathbf{M} is almost surely invertible. By letting $\tilde{\alpha} = \alpha \mathbf{M}^{\frac{1}{2}}$ and $\tilde{\mathbf{m}} = \mathbf{M}^{-\frac{1}{2}} \mathbf{m}$, we have

$$\gamma_0 = \frac{\tilde{\alpha} \tilde{\mathbf{m}} \tilde{\mathbf{m}}^H \tilde{\alpha}^H}{\tilde{\alpha} \tilde{\mathbf{M}} \tilde{\alpha}^H}, \quad (38)$$

where γ_0 is maximized when $\tilde{\alpha} = \tilde{\mathbf{m}} \tilde{\mathbf{M}}^{-1}$ for $\tilde{c} \neq 0$ according to Cauchy-Schwartz inequality. The optimal α is given by

$$\alpha = \tilde{\mathbf{m}} \tilde{\mathbf{M}}^{-1} = \frac{c \mathbf{m}^H \mathbf{M}^{-1}}{1 + \mathbf{m}^H \mathbf{M}^{-1} \mathbf{m}} \stackrel{(a)}{=} c \mathbf{m}^H (\mathbf{M} + \mathbf{m} \mathbf{m}^H)^{-1}, \quad (39)$$

where $c = \tilde{c}(1 + \mathbf{m}^H \mathbf{M}^{-1} \mathbf{m})$ and step (a) follows from Lemma 1. Thus we proved (18). Since (17) is convex, by setting the derivative of the optimization objective w.r.t. α to be to 0, we can obtain that α^{opt} is the optimal solution when $c = 1$. Therefore, we complete the proof of Proposition 1. \square

APPENDIX B PROOF OF THEOREM 1

According to Lemma 1, we can write

$$\mathbf{D}_r = \mathbf{Q} \mathbf{D}_{h,0} \mathbf{L} \mathbf{F}, \quad (40)$$

where

$$\begin{aligned} \mathbf{Q} &= \text{diag}(\mathbf{Q}_k; k \in [K]), \quad \mathbf{Q}_k = \left(\frac{\hat{\mathbf{H}}_k \hat{\mathbf{H}}_k^H}{N_k} + \mathbf{Z}_k + \rho_k \mathbf{I}_{N_k} \right)^{-1}, \\ \mathbf{L} &= \text{diag}(N_k^{-1}; k \in [K]), \quad \mathbf{D}_{h,0} = \text{diag}(\hat{\mathbf{h}}_{0k}; k \in [K]) \\ \mathbf{F} &= \text{diag}\left((1 + \frac{1}{N_k} \hat{\mathbf{h}}_{0k}^H \mathbf{Q}_k \hat{\mathbf{h}}_{0k})^{-1}; k \in [K]\right). \end{aligned} \quad (41)$$

We first analyze the LFSC case. By setting $a = 1$, $\mathbf{m} = \mathbf{D}_r^H \hat{\mathbf{h}}_0$, and $\mathbf{M} = \mathbf{D}_r^H (\hat{\mathbf{H}} \hat{\mathbf{H}}^H + \mathbf{D}_W + \sigma^2 \mathbf{I}_N) \mathbf{D}_r$ in Lemma 1 and using (40), we can obtain

$$\gamma^{\text{lfsc}} = \frac{|\mathbf{g}^H \mathbf{G}_{\Delta_I}^{-1} \tilde{\mathbf{g}}|^2}{\mathbf{g}^H \mathbf{G}_{\Delta_I}^{-1} \mathbf{G}_{\Delta} \mathbf{G}_{\Delta_I}^{-1} \mathbf{g}}, \quad (42)$$

where

$$\begin{aligned} \mathbf{g}^H &= \hat{\mathbf{h}}_0^H \mathbf{Q} \mathbf{D}_{h,0} \mathbf{L}, \quad \tilde{\mathbf{g}}^H = \tilde{\mathbf{h}}_0^H \mathbf{Q} \mathbf{D}_{h,0} \mathbf{L}, \\ \mathbf{G}_{\Delta_I} &= \mathbf{L} \mathbf{D}_{h,0}^H \mathbf{Q} (\hat{\mathbf{H}} \hat{\mathbf{H}}^H + \mathbf{D}_W + \sigma^2 \mathbf{I}_N) \mathbf{Q} \mathbf{D}_{h,0} \mathbf{L}, \\ \mathbf{G}_{\Delta} &= \mathbf{L} \mathbf{D}_{h,0}^H \mathbf{Q} (\tilde{\mathbf{H}} \tilde{\mathbf{H}}^H + \mathbf{W} + \sigma^2 \mathbf{I}_N) \mathbf{Q} \mathbf{D}_{h,0} \mathbf{L}. \end{aligned} \quad (43)$$

It can be proved that $\|\mathbf{Q}\| \leq \sup_k \|\mathbf{Q}_k\| = \frac{1}{\min_k \rho_k}$ for $\rho_k > 0$. According to Lemma 2 and 3, we have

$$\begin{aligned} [\mathbf{g}]_k - \frac{\text{Tr}[\Phi_0]_{[k,k]} \Theta_k}{N_k} &= \frac{\hat{\mathbf{h}}_{0k}^H \mathbf{Q}_k \hat{\mathbf{h}}_{0k}}{N_k} - \frac{\text{Tr}[\Phi_0]_{[k,k]} \Theta_k}{N_k} \\ &= \frac{\mathbf{q}_0^H (\Phi_{0k}^{\frac{1}{2}})^H \mathbf{Q}_k \Phi_{0k}^{\frac{1}{2}} \mathbf{q}_0}{N_k} - \frac{\text{Tr}(\Phi_{0k}^{\frac{1}{2}})^H \mathbf{Q}_k \Phi_{0k}^{\frac{1}{2}}}{N_k} \\ &+ \frac{\text{Tr}[\Phi_0]_{[k,k]} \mathbf{Q}_k}{N_k} - \frac{\text{Tr}[\Phi_0]_{[k,k]} \Theta_k}{N_k} \xrightarrow[N \xrightarrow{c_1, \dots, c_K} \rightarrow \infty]{a.s.} 0, \end{aligned} \quad (44)$$

where $\mathbf{q}_0 \sim \mathcal{CN}(0, \mathbf{I}_N)$ and $\Phi_{0k}^{\frac{1}{2}} = \Phi_0^{\frac{1}{2}}[\mathbf{s}_k, :] \in \mathbb{C}^{N_k \times N}$. Since K is a given number, it holds true that $[\mathbf{g}]_k - [\mathbf{v}]_k$ converges to 0 almost surely for each $k \in [K]$. Similarly, we write

$$\begin{aligned} [\mathbf{G}_{\Delta}]_{k,l} &= \frac{\hat{\mathbf{h}}_{0k}^H \mathbf{Q}_k ([\mathbf{W}]_{[k,l]} + \sigma^2 \mathbb{I}_{\{k=l\}} \mathbf{I}_{N_k}) \mathbf{Q}_l \hat{\mathbf{h}}_{0l}}{N_k N_l} \\ &+ \frac{\hat{\mathbf{h}}_{0k}^H \mathbf{Q}_k \tilde{\mathbf{H}}_k \tilde{\mathbf{H}}_l^H \mathbf{Q}_l \hat{\mathbf{h}}_{0l}}{N_k N_l} = G_{kl,1} + G_{kl,2}. \end{aligned} \quad (45)$$

According to [32, Theorem 2], we can conclude that the spectral norm of matrix $\frac{1}{\sqrt{N_k}} \tilde{\mathbf{H}}_k$ is bounded with probability 1 for each $k \in [K]$ such that the following holds almost surely

$$\sup_{N \geq 1} \left\| \frac{\mathbf{Q}_k \tilde{\mathbf{H}}_k \tilde{\mathbf{H}}_l^H \mathbf{Q}_l}{\sqrt{N_k N_l}} \right\| \leq \sup_{N \geq 1} \frac{\|\tilde{\mathbf{H}}_k\| \|\tilde{\mathbf{H}}_l\|}{\min_k \rho_k^2} < +\infty, \quad (46)$$

for each $k, l \in [K]$. By Lemma 2 and 3, the difference $\mathcal{D}_{G_{kl,2}} = G_{kl,2} - \frac{1}{\sqrt{N_k N_l}} \bar{\Pi}_{B,kl}([\Phi_0]_{[l,k]})$ can be written as

$$\begin{aligned} \mathcal{D}_{G_{kl,2}} &= G_{kl,2} - \frac{\text{Tr} \mathbf{Q}_k \tilde{\mathbf{H}}_k \tilde{\mathbf{H}}_l^H \mathbf{Q}_l [\Phi_0]_{[l,k]}}{N_k N_l} \\ &+ \frac{\text{Tr} \mathbf{Q}_k \tilde{\mathbf{H}}_k \tilde{\mathbf{H}}_l^H \mathbf{Q}_l [\Phi_0]_{[l,k]}}{N_k N_l} - \frac{\bar{\Pi}_{B,kl}([\Phi_0]_{[l,k]})}{\sqrt{N_k N_l}}, \end{aligned} \quad (47)$$

which converges to 0 almost surely. Following a similar derivation, we can prove $G_{kl,1}$ converges almost surely to $\frac{1}{N_k N_l} \bar{\Upsilon}_{kl}([\Phi_0]_{[l,k]}, [\mathbf{W} + \sigma^2 \mathbf{I}_N]_{[k,l]})$. Moreover, it can be shown that,

$$[\tilde{\mathbf{g}}]_k - [\mathbf{v}]_k \xrightarrow[N \xrightarrow{c_1, \dots, c_K} \rightarrow \infty]{a.s.} 0, \quad (48)$$

$$[\mathbf{G}_{\Delta_I}]_{k,l} - [\mathbf{\Delta}_I]_{k,l} \xrightarrow[N \xrightarrow{c_1, \dots, c_K} \rightarrow \infty]{a.s.} 0, \quad (49)$$

for each $k, l \in [K]$. According to the continuous mapping theorem [33], we have

$$\gamma^{\text{lfsc}} \xrightarrow[N \xrightarrow{c_1, \dots, c_K} \rightarrow \infty]{a.s.} \bar{\gamma}^{\text{lfsc}}, \quad (50)$$

which concludes (25b). The proof for (25a) and (25c) can be obtained similarly and is omitted here. \square

APPENDIX C USEFUL RESULTS

In this section, we will give the main mathematical results, which will be frequently used throughout the proofs in this paper.

A. Matrix Inversion Lemma

Lemma 1. [21, Lemma 1]: Let $\mathbf{M} \in \mathbb{C}^{N \times N}$ be an invertible matrix, $\mathbf{m} \in \mathbb{C}^N$, and $a \in \mathbb{C}$. If $1 + a\mathbf{m}^H \mathbf{M}^{-1} \mathbf{m} \neq 0$, we have

$$\mathbf{m}^H (\mathbf{M} + a\mathbf{m}\mathbf{m}^H)^{-1} = \frac{\mathbf{m}^H \mathbf{M}^{-1}}{1 + a\mathbf{m}^H \mathbf{M}^{-1} \mathbf{m}}. \quad (51)$$

B. Convergence of Random Vectors

Lemma 2. [21, Lemma 4]: Let $\mathbf{A}_N \in \mathbb{C}^{N \times N}$ be a random matrix and $\mathbf{x}_N \in \mathbb{C}^N$ be a random vector with i.i.d. entries with normalized Gaussian distribution $\mathcal{CN}(0, 1)$. Assume that for each j , $[\mathbf{x}]_j$ is independent with sequence $(\mathbf{A}_N)_{N \geq 1}$ and $\mathbb{P}(\sup_{N \geq 1} \|\mathbf{A}_N\| < +\infty) = 1$. Then, we have

$$\frac{\text{Tr}(\mathbf{x}_N^H \mathbf{A}_N \mathbf{x}_N)}{N} - \frac{\text{Tr} \mathbf{A}_N}{N} \xrightarrow[N \rightarrow +\infty]{a.s.} 0. \quad (52)$$

Proof: Here we provide a proof different from [21] which relies on Tonelli's theorem. To describe independence, [21] assumes the underlying probability space is the product probability space of $(\mathbf{x}_N)_{N \geq 1}$ and $(\mathbf{A}_N)_{N \geq 1}$, whereas here we discuss within the same probability space.

Denoting the underline probability space $(\Omega, \mathcal{F}, \mathbb{P})$. Define the set $A_{n,K} = \{\omega \in \Omega : \sup_{j \geq n} \|\mathbf{A}_j(\omega)\| \leq K\}$ and $B_{N,\epsilon} = \{\omega \in \Omega : d_N(\omega) \leq \epsilon\}$, where

$$d_N(\omega) = \left| \frac{\text{Tr}[\mathbf{x}_N^H(\omega) \mathbf{A}_N(\omega) \mathbf{x}_N(\omega)]}{N} - \frac{\text{Tr} \mathbf{A}_N(\omega)}{N} \right|. \quad (53)$$

To prove $d_N \xrightarrow[N \rightarrow +\infty]{a.s.} 0$, we only need to show that for any positive integer n and $\epsilon > 0$, $\mathbb{P}(\bigcup_{n=1}^{+\infty} \bigcap_{N=n}^{+\infty} B_{N,\epsilon}) = 1$ holds. In the following, we will prove this by a stronger result $\mathbb{P}(\bigcup_{n=1}^{+\infty} \bigcap_{N=n}^{+\infty} B_{N,\epsilon}) \geq 1$. To this end, we write

$$\begin{aligned} \mathbb{P}(\bigcup_{n=1}^{+\infty} \bigcap_{N=n}^{+\infty} B_{N,\epsilon}) &\geq \mathbb{P}(\bigcup_{n=1}^{+\infty} \bigcap_{N=n}^{+\infty} B_{N,\epsilon} \bigcap \bigcup_{K=0}^{+\infty} A_{n,K}) \\ &= \mathbb{P}(\bigcup_{K=0}^{+\infty} \bigcup_{n=1}^{+\infty} \bigcap_{N=n}^{+\infty} B_{N,\epsilon} \bigcap A_{n,K}) \\ &\stackrel{(a)}{=} \lim_{K \rightarrow +\infty} \lim_{n \rightarrow +\infty} \mathbb{P}(\bigcap_{N=n}^{+\infty} B_{N,\epsilon} \bigcap A_{n,K}), \end{aligned} \quad (54)$$

where step (a) follows from $A_{n,K} \subset A_{n,K+1}$, $A_{n,K} \subset A_{n+1,K}$, and continuity of probability measure. On the other side, we have

$$\begin{aligned} \mathbb{P}(\bigcap_{N=n}^{+\infty} B_{N,\epsilon} \bigcap A_{n,K}) &= 1 - \mathbb{P}(\bigcup_{N=n}^{+\infty} B_{N,\epsilon}^c \bigcup A_{n,K}^c) \\ &= 1 - \mathbb{P}(A_{n,K}^c) - \mathbb{P}(\bigcup_{N=n}^{+\infty} B_{N,\epsilon}^c \bigcap A_{n,K}) \\ &\geq \mathbb{P}(A_{n,K}) - \sum_{N \geq n} \mathbb{P}(B_{N,\epsilon}^c \bigcap A_{n,K}). \end{aligned} \quad (55)$$

TABLE II
TABLE OF NOTATIONS

Notation	Expression
$F_k(\mathcal{A})$	$\text{Tr} \mathbf{A} \mathbf{Q}_k$
$\Phi_{B,kl}(\mathcal{A}, \mathbf{b})$	$\text{Tr} \mathbf{A} \mathbf{Q}_k \mathbf{X}_k \text{diag}(\mathbf{b}) \mathbf{Y}_l^H$
$\Phi_{kl}(\mathcal{A}, \mathbf{b})$	$\text{Tr} \mathbf{A} \mathbf{Q}_k \mathbf{X}_k \text{diag}(\mathbf{b}) \mathbf{X}_l^H$
$\Upsilon_{kl}(\mathcal{A}, \mathcal{B})$	$\text{Tr} \mathbf{A} \mathbf{Q}_k \mathcal{B} \mathbf{Q}_l$
$\Pi_{B,kl}(\mathcal{A})$	$\text{Tr} \mathbf{A} \mathbf{Q}_k \mathbf{Y}_k \mathbf{Y}_l^H \mathbf{Q}_l$
$\Pi_{kl}(\mathcal{A})$	$\text{Tr} \mathbf{A} \mathbf{Q}_k \mathbf{X}_k \mathbf{X}_l^H \mathbf{Q}_l$

By using Markov's inequality, we can get

$$\begin{aligned} \mathbb{P}(B_{N,\epsilon}^c \bigcap A_{n,K}) &= \mathbb{E} [\mathbb{I}_{\{d_N \geq \epsilon\}} \mathbb{I}_{A_{n,K}}] \\ &\leq \mathbb{E} [\mathbb{I}_{\{d_N \geq \epsilon\}} \mathbb{I}_{\{\|\mathbf{A}_N\| \leq K\}}] \\ &\leq \mathbb{E} [\mathbb{I}_{\{\|\mathbf{A}_N\| \leq K\}}] \mathbb{E} (\epsilon^{-p} d_N^p | \mathbf{A}_N) \\ &\stackrel{(a)}{\leq} C_p N^{-\frac{p}{2}} \mathbb{E} [\mathbb{I}_{\{\|\mathbf{A}_N\| \leq K\}} \|\mathbf{A}_N\|^p] \\ &= \mathcal{O}(N^{-\frac{p}{2}} K^p), \end{aligned} \quad (56)$$

where $p > 2$, C_p is a constant, and step (a) follows from the trace lemma [21, Lemma 3]. Hence, $\sum_{N=n}^{+\infty} \mathbb{P}(B_{N,\epsilon}^c \bigcap A_{n,K}) \rightarrow 0$ as $n \rightarrow +\infty$ and it holds true that

$$\lim_{n \rightarrow +\infty} \mathbb{P}(\bigcap_{N=n}^{+\infty} B_{N,\epsilon} \bigcap A_{n,K}) \geq \lim_{n \rightarrow +\infty} \mathbb{P}(A_{n,K}). \quad (57)$$

By combining (57) and (54), we can obtain

$$\begin{aligned} \mathbb{P}(\bigcup_{n=1}^{+\infty} \bigcap_{N=n}^{+\infty} B_{N,\epsilon}) &\geq \lim_{K \rightarrow +\infty} \lim_{n \rightarrow +\infty} \mathbb{P}(A_{n,K}) \\ &\stackrel{(a)}{=} \mathbb{P}(\bigcup_{k=0}^{+\infty} \bigcup_{n=1}^{+\infty} A_{n,K}) = \mathbb{P}(\bigcup_{n=1}^{+\infty} \bigcup_{K=0}^{+\infty} A_{n,K}) \stackrel{(b)}{=} 1, \end{aligned} \quad (58)$$

where step (a) follows from continuity of probability measure and step (b) follows from the identity $\mathbb{P}(\bigcup_{K=0}^{+\infty} A_{n,K}) = 1$. This completes the proof of Lemma 2. \square

C. Convergence of Random Matrices

The SINR involves terms associated with random matrices $\hat{\Sigma}$ and $\tilde{\Sigma}$ whose columns are generally correlated. This makes the evaluation of the SINR very challenging. In the following, we introduce a more general setting and provide the relevant results, which can be utilized to prove Theorem 1.

Let $\tilde{\mathbf{X}} = [\mathbf{A}_1 \mathbf{x}_1, \dots, \mathbf{A}_M \mathbf{x}_M] \in \mathbb{C}^{N \times M}$ and $\tilde{\mathbf{Y}} = [\mathbf{B}_1 \mathbf{x}_1, \dots, \mathbf{B}_M \mathbf{x}_M] \in \mathbb{C}^{N \times M}$, where $\mathbf{A}_j, \mathbf{B}_j \in \mathbb{C}^{N \times N_i^x}$, and $\mathbf{x}_j \sim \mathcal{CN}(0, \mathbf{I}_{N_i^x})$ for each $j \in [M]$. Define two correlation matrices sets $A = \{\mathbf{A}_j : j \in [M]\}$ and $B = \{\mathbf{B}_j : j \in [M]\}$. Denote $\Omega_j = \mathbf{A}_j \mathbf{A}_j^H$, $\mathbf{A}_{jk} = \mathbf{A}_j[\mathbf{s}_k, :]$, and $\mathbf{B}_{jk} = \mathbf{B}_j[\mathbf{s}_k, :]$. Let $\mathbf{X}_k = \frac{1}{\sqrt{N_k}} \tilde{\mathbf{X}}[\mathbf{s}_k, :]$ and $\mathbf{Y}_k = \frac{1}{\sqrt{N_k}} \tilde{\mathbf{Y}}[\mathbf{s}_k, :]$. The resolvent matrix of $\mathbf{X}_k \mathbf{X}_k^H + \mathbf{S}_k$ is given by

$$\mathbf{Q}_k(z) = (\mathbf{X}_k \mathbf{X}_k^H + \mathbf{S}_k - z \mathbf{I}_{N_k})^{-1}, \quad (59)$$

with \mathbf{S}_k being deterministic and Hermitian nonnegative. We further define some functions of the resolvents in Table II, where we set $\mathbf{Q}_k = \mathbf{Q}_k(z_k)$, for each $k \in [K]$ and omit the variable z_k for the sake of notation simplicity. Furthermore, \mathcal{A} and \mathcal{B} are appropriately sized matrices, and \mathbf{b} is a properly dimensioned vector. We next introduce the stochastic equivalent notation.

Definition 1. (Stochastic Equivalent) For random sequence $(X_N)_{N \geq 1}$ and deterministic sequence $(\bar{X}_N)_{N \geq 1}$, we use

$X_N \asymp_l \bar{X}_N$ to denote

$$|\mathbb{E}X_N - \bar{X}_N| = \mathcal{O}(N^{-l}), \quad \frac{|X_N - \bar{X}_N|}{N} \xrightarrow[N \rightarrow +\infty]{a.s.} 0. \quad (60)$$

The following lemma gives the stochastic equivalents for the functions in Table II.

Lemma 3. Assume Assumption A.1 holds, the maximal spectral norm of the correlation matrices is bounded, i.e., $\limsup_N \max_{j \in [M]} \{\|\mathbf{A}_j\|, \|\mathbf{B}_j\|\} < +\infty$, and the spectral norms of matrices \mathbf{A}, \mathbf{B} and $\text{diag}(\mathbf{b})$ are uniformly bounded. For any $z_1, \dots, z_K < 0$, we have $F_k \asymp_{\frac{1}{2}} \bar{F}_k$, $\Phi_{B,kl} \asymp_{\frac{1}{2}} \bar{\Phi}_{B,kl}$, $\Phi_{kl} \asymp_{\frac{1}{2}} \bar{\Phi}_{kl}$, $\Upsilon_{kl} \asymp_{\frac{1}{2}} \bar{\Upsilon}_{kl}$, $\Pi_{B,kl} \asymp_{\frac{1}{2}} \bar{\Pi}_{B,kl}$, and $\Pi_{kl} \asymp_{\frac{1}{2}} \bar{\Pi}_{kl}$, where

$$\bar{F}_k(\mathbf{A}) = \text{Tr} \mathbf{A} \boldsymbol{\Theta}_k, \quad (61)$$

$$\bar{\Phi}_{B,kl}(\mathbf{A}, \mathbf{b}) = \frac{\sum_{j=1}^M [\tilde{\mathbf{F}}_k \mathbf{b}]_j \text{Tr} \mathbf{A} \boldsymbol{\Theta}_k \mathbf{A}_{jk} \mathbf{B}_{jl}^H}{\sqrt{N_k N_l}}, \quad (62)$$

$$\bar{\Upsilon}_{kl}(\mathbf{A}, \mathbf{B}) = \text{Tr} \mathbf{A} \boldsymbol{\Theta}_k \mathbf{B} \boldsymbol{\Theta}_l + \tilde{\lambda}_{kl}(\mathbf{A}) \tilde{\mathbf{F}}_k \tilde{\mathbf{F}}_l \Xi_{kl} \lambda_{kl}(\mathbf{B}), \quad (63)$$

and $\bar{\Pi}_{kl,B}$ is given at the top of the next page. Functions $\bar{\Phi}_{kl}$ and $\bar{\Pi}_{kl}$ can be obtained by setting $\mathbf{B}_j = \mathbf{A}_j$ for each $j \in [M]$ in $\bar{\Phi}_{kl,B}$ and $\bar{\Pi}_{kl,B}$, respectively and we omit them here. The deterministic variables are defined in Table III where P and O can be any symbol from the set $\{A, B\}$. The matrix $\boldsymbol{\Theta}_k$ is defined by the positive solutions of the following system of equations w.r.t. δ_{jk}

$$\delta_{jk} = \frac{1}{N_k} \text{Tr}[\boldsymbol{\Omega}_j]_{[k,k]} \boldsymbol{\Theta}_k, j \in [M], \quad (65)$$

$$\boldsymbol{\Theta}_k = \left(-z_k \mathbf{I}_{N_k} + \mathbf{S}_k + \frac{1}{N_k} \sum_{j=1}^M \frac{[\boldsymbol{\Omega}_j]_{[k,k]}}{1 + \delta_{jk}} \right)^{-1}. \quad (66)$$

Proof: The proof of Lemma 3 is given in Appendix D. \square

APPENDIX D PROOF OF LEMMA 3

The proof relies on Gaussian tools [16], [34]–[37], which consist of the integration by parts formula [35, Eq. (17)] and the Poincaré-Nash inequality [35, Eq. (18)]. According to the Poincaré-Nash inequality, the variance of functions defined in Table II can be proved of order $\mathcal{O}(1)$ (See [32, Lemma 9] for the case of F_k and the proof of other functions are similar). As a result, for given $\epsilon > 0$, we have

$$\sum_{N=1}^{+\infty} \mathbb{P} \left(\frac{|\mathcal{X} - \mathbb{E}\mathcal{X}|}{N} \geq \epsilon \right) \leq \sum_{N=1}^{+\infty} \frac{\text{Var}(\mathcal{X})}{\epsilon^2 N^2} < +\infty, \quad (67)$$

where \mathcal{X} can be any function in Table II. Thus, according to Borel-Cantelli lemma, we have

$$\frac{\mathcal{X} - \mathbb{E}\mathcal{X}}{N} \xrightarrow[N \xrightarrow{c_1, \dots, c_K} +\infty]{a.s.} 0. \quad (68)$$

Therefore, to show the stochastic equivalence, we only need to evaluate the means of functions in Table II.

A. Evaluation of $\mathbb{E}F_k$

Before delving into the details of the proof, we first define the following quantities

$$\alpha_{jk} = \frac{1}{N_k} \text{Tr}[\boldsymbol{\Omega}_s]_{[k,k]} \mathbf{Q}_k, \quad \mathbf{D}_{\alpha,k} = \text{diag}(\alpha_{jk}; j \in [M]),$$

$$\tilde{\mathbf{F}}_{\alpha,k} = (\mathbf{I} + \mathbb{E} \mathbf{D}_{\alpha,k})^{-1},$$

$$\boldsymbol{\Theta}_{\alpha,k} = \left(-z \mathbf{I}_{N_k} + \mathbf{S}_k + \frac{1}{N_k} \sum_{j=1}^M \frac{[\boldsymbol{\Omega}_j]_{[k,k]}}{1 + \alpha_{jk}} \right)^{-1}. \quad (69)$$

These quantities will serve as intermediate variables in the proof, i.e., we will show $\mathbf{Q}_k \approx \boldsymbol{\Theta}_{\alpha,k} \approx \boldsymbol{\Theta}_k$.

Applying integration by parts formula to $\mathbb{E}[\mathbf{Q}_k]_{i,p}[\mathbf{x}_s]_a[\mathbf{Y}_l]_{j,s}^*$ and taking $[\mathbf{x}_s]_a$ as the variable, we have

$$\begin{aligned} \mathbb{E}[\mathbf{Q}_k]_{i,p}[\mathbf{x}_s]_a[\mathbf{Y}_l]_{j,s}^* &= \mathbb{E} \frac{\partial[\mathbf{Q}_k]_{i,p}[\mathbf{Y}_l]_{j,s}^*}{\partial[\mathbf{x}_s]_a} \\ &= \mathbb{E} - \frac{1}{\sqrt{N_k}} [\mathbf{Q}_k \mathbf{X}_k]_{i,s} [\mathbf{A}_{sk}^H \mathbf{Q}_k]_{a,p} [\mathbf{Y}_l]_{j,s}^* \\ &\quad + \mathbb{E} \frac{1}{\sqrt{N_l}} [\mathbf{Q}_k]_{i,p} [\mathbf{B}_{sl}^H]_{a,j}. \end{aligned} \quad (70)$$

Multiplying $\frac{1}{\sqrt{N_k}} [\mathbf{A}_{sk}]_{p,a}$ at both sides of (70) and summing over the subscripts p and a , the following holds

$$\begin{aligned} \mathbb{E}[\mathbf{Q}_k \mathbf{X}_k]_{i,s} [\mathbf{Y}_l]_{j,s}^* &= \mathbb{E} \frac{[\mathbf{Q}_k \mathbf{A}_{sk} \mathbf{B}_{sl}^H]_{i,j}}{\sqrt{N_k N_l}} \\ &\quad - \mathbb{E} \alpha_{sk} [\mathbf{Q}_k \mathbf{X}_k]_{i,s} [\mathbf{Y}_l]_{j,s}^*. \end{aligned} \quad (71)$$

By writing the random variable α_{sk} as the sum of its mean and its centered version, i.e., $\alpha_{sk} = \bar{\alpha}_{sk} + \hat{\alpha}_{sk}$ and solving (71) w.r.t. $\mathbb{E}[\mathbf{Q}_k \mathbf{X}_k]_{i,s} [\mathbf{Y}_l]_{j,s}^*$, we get

$$\begin{aligned} \mathbb{E}[\mathbf{Q}_k \mathbf{X}_k]_{i,s} [\mathbf{Y}_l]_{j,s}^* &= \mathbb{E} \frac{[\mathbf{Q}_k \mathbf{A}_{sk} \mathbf{B}_{sl}^H]_{i,j}}{\sqrt{N_k N_l} (1 + \bar{\alpha}_{sk})} \\ &\quad - \mathbb{E} \frac{\hat{\alpha}_{sk}}{1 + \bar{\alpha}_{sk}} [\mathbf{Q}_k \mathbf{X}_k]_{i,s} [\mathbf{Y}_l]_{j,s}^*. \end{aligned} \quad (72)$$

(72) will also be used for the evaluation of $\mathbb{E}\Phi_{B,kl}$ later. To obtain the approximation of the trace of the resolvent, we set $l = k$ and $\mathbf{Y}_k = \mathbf{X}_k$, i.e., $\mathbf{B}_s = \mathbf{A}_s$, $\forall s \in [M]$. By summing over the subscript s , we can obtain

$$\begin{aligned} \mathbb{E}[\mathbf{Q}_k \mathbf{X}_k \mathbf{X}_k^H]_{i,j} &= \mathbb{E}[\mathbf{Q}_k \sum_{s=1}^M \frac{[\boldsymbol{\Omega}_s]_{[k,k]}}{N_k (1 + \bar{\alpha}_{sk})}]_{i,j} \\ &\quad - \mathbb{E}[\mathbf{Q}_k \mathbf{X}_k \mathbf{D}_{\alpha,k} \tilde{\mathbf{F}}_{\alpha,k} \mathbf{X}_k^H]_{i,j}. \end{aligned} \quad (73)$$

By using the resolvent identity $\mathbf{Q}_k \mathbf{X}_k \mathbf{X}_k^H = z_k \mathbf{Q}_k - \mathbf{Q}_k \mathbf{S}_k + \mathbf{I}_{N_k}$ on $\mathbb{E}[\mathbf{Q}_k \mathbf{X}_k \mathbf{X}_k^H]_{i,j}$, multiplying both sides $[\boldsymbol{\Theta}_{\alpha,k} \mathbf{A}]_{j,i}$, and summing over the subscripts i and j , we can get

$$\begin{aligned} \mathbb{E} \text{Tr} \mathbf{A} \mathbf{Q}_k - \text{Tr} \mathbf{A} \boldsymbol{\Theta}_{\alpha,k} &= \mathbb{E} \text{Tr} \mathbf{Q}_k \mathbf{X}_k \mathbf{D}_{\alpha,k} \tilde{\mathbf{F}}_{\alpha,k} \mathbf{X}_k^H \boldsymbol{\Theta}_{\alpha,k} \mathbf{A} := \varepsilon_k(\mathbf{A}). \end{aligned} \quad (74)$$

We can write the residual term $\varepsilon_k(\mathbf{A})$ as

$$\begin{aligned} \varepsilon_k(\mathbf{A}) &= \sum_{j=1}^M \mathbb{E} \hat{\alpha}_{jk} \underbrace{[\tilde{\mathbf{F}}_{\alpha,k} \mathbf{X}_k^H \boldsymbol{\Theta}_{\alpha,k} \mathbf{A} \mathbf{Q}_k \mathbf{X}_k]_{j,j}}_{:= \chi_{jk}} \\ &\stackrel{(a)}{\leq} \sum_{j=1}^M \text{Var}^{\frac{1}{2}}(\alpha_{jk}) \text{Var}^{\frac{1}{2}}(\chi_{jk}) \stackrel{(b)}{=} \mathcal{O}(\frac{1}{N^{\frac{1}{2}}}), \end{aligned} \quad (75)$$

where step (a) follows from Cauchy-Schwartz inequality. Step (b) follows from the fact $\text{Var}(\alpha_{jk}) = \mathcal{O}(\frac{1}{N^2})$ and $\text{Var}(\chi_{jk}) = \mathcal{O}(\frac{1}{N})$, which can be proved by Poincaré-Nash inequality. Hence, we build the relation between \mathbf{Q}_k and $\boldsymbol{\Theta}_{\alpha,k}$.

To establish the relationship between $\boldsymbol{\Theta}_{\alpha,k}$ and $\boldsymbol{\Theta}_k$, we take the difference between $\text{Tr}[\boldsymbol{\Omega}_j]_{[k,k]} \boldsymbol{\Theta}_{\alpha,k}$ and δ_{jk} for each $j \in [M]$. Following the same procedure as in the proof of [32, Proposition 3], we can show that $|\text{Tr} \mathbf{A} \boldsymbol{\Theta}_k - \text{Tr} \mathbf{A} \boldsymbol{\Theta}_{\alpha,k}| =$

TABLE III
TABLE OF DETERMINISTIC QUANTITIES

Notation	Expression	Notation	Expression
$\tilde{\mathbf{F}}_k$	$\text{diag} \left((1 + \delta_{jk})^{-1}; j \in [M] \right)$	$[\mathbf{\Gamma}_{kl}]_{i,j}$	$\frac{1}{N_k N_l} \text{Tr}[\mathbf{\Omega}_i]_{[l,k]} \mathbf{\Theta}_k [\mathbf{\Omega}_j]_{[k,l]} \mathbf{\Theta}_l$
$\tilde{\mathbf{\Xi}}_{kl}$	$(\mathbf{I}_M - \mathbf{\Gamma}_{kl} \tilde{\mathbf{F}}_k \tilde{\mathbf{F}}_l)^{-1}$	$\tilde{\lambda}_{kl}(\mathcal{A})$	$\frac{1^T}{\sqrt{N_k N_l}} \text{diag} \left(\text{Tr} \mathcal{A} \mathbf{\Theta}_k [\mathbf{\Omega}_j]_{[k,l]} \mathbf{\Theta}_l; j \in [M] \right)$
$\tilde{\lambda}_{P,O,kl}(\mathcal{A})$	$\frac{1^T}{\sqrt{N_k N_l}} \text{diag} \left(\text{Tr} \mathcal{A} \mathbf{\Theta}_k \mathbf{P}_{jk} \mathbf{O}_{jl}^H \mathbf{\Theta}_l; j \in [M] \right)$	$\lambda_{kl}(\mathcal{B})$	$\frac{1}{\sqrt{N_k N_l}} \text{diag} \left(\text{Tr} [\mathbf{\Omega}_j]_{[l,k]} \mathbf{\Theta}_k \mathcal{B} \mathbf{\Theta}_l; j \in [M] \right) \mathbf{1}_M$
$[\mathbf{A}_{P,O,kl}]_{i,j}$	$\frac{1}{N_k N_l} \text{Tr}[\mathbf{\Omega}_i]_{[l,k]} \mathbf{\Theta}_k \mathbf{P}_{jk} \mathbf{O}_{jl}^H \mathbf{\Theta}_l$	$\mathbf{D}_{P,O,k}$	$\frac{1}{N_k} \text{diag} \left(\text{Tr} \mathbf{P}_{jk} \mathbf{O}_{jl}^H \mathbf{\Theta}_k; j \in [M] \right)$

$$\begin{aligned} \tilde{\Pi}_{kl,B}(\mathcal{A}) &= \left[\tilde{\lambda}_{B,B,kl}(\mathcal{A}) - \tilde{\lambda}_{B,A,kl}(\mathcal{A}) \mathbf{D}_{A,B,l} \tilde{\mathbf{F}}_l - \tilde{\lambda}_{A,B,kl}(\mathcal{A}) \mathbf{D}_{B,A,k} \tilde{\mathbf{F}}_k \right] \mathbf{1}_M \\ &\quad + \tilde{\lambda}_{kl}(\mathcal{A}) \tilde{\mathbf{F}}_k \tilde{\mathbf{F}}_l \tilde{\mathbf{\Xi}}_{kl} \left[\mathbf{\Lambda}_{B,B,kl} - \mathbf{\Lambda}_{B,A,kl} \mathbf{D}_{A,B,l} \tilde{\mathbf{F}}_l - \mathbf{\Lambda}_{A,B,kl} \mathbf{D}_{B,A,k} \tilde{\mathbf{F}}_k + \mathbf{D}_{B,A,k} \mathbf{D}_{A,B,l} \right] \mathbf{1}_M. \end{aligned} \quad (64)$$

$\mathcal{O}(N^{-\frac{1}{2}})$, which concludes (61).

B. Evaluation of $\mathbb{E}\Phi_{B,kl}$

Multiplying $[\mathbf{b}]_s$ and $[\mathcal{A}]_{j,i}$ at both sides of (72) and summing over the subscripts s, i , and j , we can obtain

$$\begin{aligned} \mathbb{E}\Phi_{B,kl}(\mathcal{A}, \mathbf{b}) &= -\mathbb{E}[\mathbf{Q}_k \mathbf{X}_k \text{diag}(\mathbf{b}) \tilde{\mathbf{D}}_{\alpha,k} \tilde{\mathbf{F}}_{\alpha,k} \mathbf{Y}_l^H] \\ &\quad + \sum_s \frac{[\mathbf{b}]_s \text{Tr} \mathcal{A} (\mathbb{E} \mathbf{Q}_k) \mathbf{A}_{sk} \mathbf{B}_{sl}^H}{\sqrt{N_k N_l} (1 + \underline{\alpha}_{sk})} \\ &\stackrel{(a)}{=} \sum_s \frac{[\mathbf{b}]_s \text{Tr} \mathcal{A} \mathbf{\Theta}_k \mathbf{A}_{sk} \mathbf{B}_{sl}^H}{\sqrt{N_k N_l} (1 + \delta_{sk})} + \mathcal{O}(N^{-\frac{1}{2}}), \end{aligned} \quad (76)$$

where step (a) follows from (61) and the variance control.

C. Evaluation of $\mathbb{E}\Upsilon_{kl}$

According to integration by parts formula, we get

$$\begin{aligned} \mathbb{E}[\mathbf{Q}_k \mathcal{B} \mathbf{Q}_l \mathbf{X}_l]_{i,s} [\mathbf{X}_l]_{j,s}^* &= \mathbb{E} \frac{[\mathbf{Q}_k \mathcal{B} \mathbf{Q}_l [\mathbf{\Omega}_s]_{[l,l]}]_{i,j}}{N_l (1 + \underline{\alpha}_{sl})} \\ &\quad - \mathbb{E} \frac{\dot{\alpha}_{sl}}{1 + \underline{\alpha}_{sl}} [\mathbf{Q}_k \mathcal{B} \mathbf{Q}_l \mathbf{X}_l]_{i,s} [\mathbf{X}_l]_{j,s}^* \\ &\quad - \frac{\mathbb{E}\Upsilon_{kl}([\mathbf{\Omega}_s]_{[l,k]}, \mathcal{B}) [\mathbf{Q}_k \mathbf{X}_k]_{i,s} [\mathbf{X}_l]_{j,s}^*}{\sqrt{N_l N_k} (1 + \underline{\alpha}_{sl})}. \end{aligned} \quad (77)$$

Summing over the subscript s and using the resolvent identity $\mathbf{Q}_l \mathbf{X}_l \mathbf{X}_l^H = \mathbf{z}_l \mathbf{Q}_l - \mathbf{Q}_l \mathbf{S}_l + \mathbf{I}_{N_l}$, the following holds

$$\begin{aligned} \mathbb{E}[\mathbf{Q}_k \mathcal{B} \mathbf{Q}_l \mathbf{\Theta}_{\alpha,l}^{-1}]_{i,j} &= \mathbb{E}[\mathbf{Q}_k \mathcal{B}]_{i,j} \\ &\quad + \mathbb{E}[\mathbf{Q}_k \mathbf{X}_k \mathbf{D}_{\Upsilon,kl}(\mathcal{B}) \tilde{\mathbf{F}}_{\alpha,l} \mathbf{X}_l^H]_{i,j} + [\varepsilon_{kl}]_{i,j}, \end{aligned} \quad (78)$$

where $\mathbf{D}_{\Upsilon,kl}(\mathcal{B}) = \frac{1}{\sqrt{N_k N_l}} \text{diag}(\Upsilon_{kl}([\mathbf{\Omega}_s]_{[l,k]}, \mathcal{B}); s \in [M])$ and ε_{kl} is the residual matrix. It can be proved by Poincaré–Nash inequality that $\text{Tr} \varepsilon \mathcal{C} = \mathcal{O}(N^{-\frac{1}{2}})$ for any \mathcal{C} with bounded spectral norm. Thus, we have

$$\begin{aligned} \mathbb{E}\Upsilon_{kl}(\mathcal{A}, \mathcal{B}) &= \text{Tr} \mathcal{A} (\mathbb{E} \mathbf{Q}_k) \mathcal{B} \mathbf{\Theta}_{\alpha,l} \\ &\quad + \mathbb{E} \text{Tr} \mathbf{Q}_k \mathbf{X}_k \mathbf{D}_{\Upsilon,kl}(\mathcal{B}) \tilde{\mathbf{F}}_{\alpha,l} \mathbf{X}_l^H \mathbf{\Theta}_{\alpha,l} \mathcal{A} + \mathcal{O}(N^{-\frac{1}{2}}). \end{aligned} \quad (79)$$

By replacing $\mathbf{\Theta}_{\alpha,l}$ and $\tilde{\mathbf{F}}_{\alpha,l}$ with $\mathbf{\Theta}_l$ and $\tilde{\mathbf{F}}_l$, respectively, setting $\mathcal{A} = [\mathbf{\Omega}_u]_{[l,k]}$ and $\mathcal{B} = [\mathbf{\Omega}_v]_{[k,l]}$, and using the approximation rules of $\Phi_{B,kl}$ in (62), we have

$$\begin{aligned} [\mathbf{\Upsilon}_{\Omega,kl}]_{u,v} &= N_k N_l [\mathbf{\Gamma}_{kl}]_{u,v} \\ &\quad + \sum_{j=1}^M [\mathbf{\Upsilon}_{\Omega,kl}]_{j,v} [\tilde{\mathbf{F}}_k \tilde{\mathbf{F}}_l]_{j,j} [\mathbf{\Gamma}_{kl}]_{u,j} + \mathcal{O}(N^{-\frac{1}{2}}), \end{aligned} \quad (80)$$

where $[\mathbf{\Upsilon}_{\Omega,kl}]_{u,v} = \mathbb{E} \text{Tr}[\mathbf{\Omega}_u]_{[l,k]} \mathbf{Q}_k [\mathbf{\Omega}_v]_{[k,l]} \mathbf{Q}_l$. Solving (80) w.r.t. $\mathbf{\Upsilon}_{\Omega,kl}$, we get

$$\mathbf{\Upsilon}_{\Omega,kl} = N_k N_l \tilde{\mathbf{\Xi}}_{kl} \mathbf{\Gamma}_{kl} + \mathcal{O}(N^{-\frac{1}{2}}) \mathbf{1}_M \mathbf{1}_M^T. \quad (81)$$

By following the similar method as in [32], [38], we can show that $\mathbf{I}_M - \mathbf{\Gamma}_{kl} \tilde{\mathbf{F}}_k \tilde{\mathbf{F}}_l$ is invertible and $\max_{i \in [M]} \sum_{j=1}^M |[\tilde{\mathbf{\Xi}}_{kl}]_{i,j}| = \mathcal{O}(1)$. Due to the space limitation, we omit the details. Similar to the evaluation of $\mathbf{\Upsilon}_{\Omega,kl}$, we can derive the approximation rules for $\mathbb{E}\Upsilon_{kl}(\mathcal{A}, [\mathbf{\Omega}_v]_{[k,l]})$ and $\mathbb{E}\Upsilon_{kl}([\mathbf{\Omega}_u]_{[l,k]}, \mathcal{B})$. Plugging these results in (79) yields

$$\begin{aligned} \mathbb{E} \text{Tr} \mathcal{A} \mathbf{Q}_k \mathcal{B} \mathbf{Q}_l &= \text{Tr} \mathcal{A} \mathbf{\Theta}_k \mathcal{B} \mathbf{\Theta}_l \\ &\quad + \tilde{\lambda}_{kl}(\mathcal{A}) \tilde{\mathbf{F}}_k \tilde{\mathbf{F}}_l \tilde{\mathbf{\Xi}}_{kl} \lambda_{kl}(\mathcal{B}) + \mathcal{O}(N^{-\frac{1}{2}}), \end{aligned} \quad (82)$$

which proves (63).

D. Evaluation of $\mathbb{E}\Pi_{B,kl}$

By applying integration by parts formula, we can obtain

$$\begin{aligned} \mathbb{E}[\mathbf{Y}_l^H \mathbf{Q}_l \mathcal{A} \mathbf{Q}_k]_{i,p} [\mathbf{Y}_k]_{p,i} &= \mathbb{E} \left\{ \frac{[\mathbf{B}_{ik} \mathbf{B}_{il}^H \mathbf{Q}_l \mathcal{A} \mathbf{Q}_k]_{p,p}}{\sqrt{N_k N_l}} \right. \\ &\quad - \frac{1}{\sqrt{N_k N_l}} [\mathbf{Y}_l^H \mathbf{Q}_l \mathbf{X}_l]_{i,i} [\mathbf{B}_{ik} \mathbf{A}_{il}^H \mathbf{Q}_l \mathcal{A} \mathbf{Q}_k]_{p,p} \\ &\quad \left. - \frac{1}{N_k} [\mathbf{Y}_l^H \mathbf{Q}_l \mathcal{A} \mathbf{Q}_k \mathbf{X}_k]_{i,i} [\mathbf{B}_{ik} \mathbf{A}_{ik}^H \mathbf{Q}_k]_{p,p} \right\}. \end{aligned} \quad (83)$$

Summing over the subscript p , and using the variance control and the approximation rules for Υ_{kl} , we get

$$\begin{aligned} \mathbb{E}[\mathbf{Y}_l^H \mathbf{Q}_l \mathcal{A} \mathbf{Q}_k \mathbf{Y}_k]_{i,i} &= \frac{\bar{\Upsilon}_{kl}(\mathcal{A}, \mathbf{B}_{ik} \mathbf{B}_{il}^H)}{\sqrt{N_k N_l}} \\ &\quad - \frac{\bar{\Upsilon}_{kl}(\mathcal{A}, \mathbf{B}_{ik} \mathbf{A}_{il}^H)}{\sqrt{N_k N_l}} \mathbb{E}[\mathbf{Y}_l^H \mathbf{Q}_l \mathbf{X}_l]_{i,i} \\ &\quad - \mathbb{E}[\mathbf{Y}_l^H \mathbf{Q}_l \mathcal{A} \mathbf{Q}_k \mathbf{X}_k]_{i,i} \frac{\text{Tr} \mathbf{B}_{ik} \mathbf{A}_{ik}^H \mathbf{\Theta}_k}{N_k} + \mathcal{O}(M^{-\frac{3}{2}}). \end{aligned} \quad (84)$$

Similarly, we can obtain

$$\begin{aligned} \mathbb{E}[\mathbf{Y}_l^H \mathbf{Q}_l \mathcal{A} \mathbf{Q}_k \mathbf{X}_k]_{i,i} &= \frac{\bar{\Upsilon}_{kl}(\mathcal{A}, \mathbf{A}_{ik} \mathbf{B}_{il}^H)}{\sqrt{N_k N_l} (1 + \delta_{ik})} \\ &\quad - \frac{\bar{\Upsilon}_{kl}(\mathcal{A}, [\mathbf{\Omega}_i]_{[k,l]})}{\sqrt{N_k N_l} (1 + \delta_{ik})} \mathbb{E}[\mathbf{Y}_l^H \mathbf{Q}_l \mathbf{X}_l]_{i,i} + \mathcal{O}(M^{-\frac{3}{2}}). \end{aligned} \quad (85)$$

Then, plugging (85) into (84), summing over the subscript i and using the approximation rules for $\Phi_{B,kl}$ in (62), we get (86) at the top of the next page, where $\tilde{\mathbf{\Xi}}_{kl} = \mathbf{I}_M + \tilde{\mathbf{F}}_k \tilde{\mathbf{F}}_l \tilde{\mathbf{\Xi}}_{kl} \mathbf{\Gamma}_{kl}$, and step (a) in (86) follows by the identity $\tilde{\mathbf{F}}_k \tilde{\mathbf{F}}_l \tilde{\mathbf{\Xi}}_{kl} = \tilde{\mathbf{\Xi}}_{kl} \tilde{\mathbf{F}}_k \tilde{\mathbf{F}}_l$. Therefore, we complete the proof of Lemma 3. \square

$$\begin{aligned}
\mathbb{E}\Pi_{B,kl}(\mathcal{A}) &= \sum_{i=1}^M \left\{ \left[\tilde{\lambda}_{B,B,kl}(\mathcal{A}) + \tilde{\lambda}_{kl}(\mathcal{A}) \tilde{\mathbf{F}}_k \tilde{\mathbf{F}}_l \tilde{\Xi}_{kl} \mathbf{\Lambda}_{B,B,kl} - [\mathbf{D}_{A,B,l} \tilde{\mathbf{F}}_l]_{i,i} \left(\tilde{\lambda}_{B,A,kl}(\mathcal{A}) + \tilde{\lambda}_{kl}(\mathcal{A}) \tilde{\mathbf{F}}_k \tilde{\mathbf{F}}_l \tilde{\Xi}_{kl} \mathbf{\Lambda}_{B,A,kl} \right) \right. \right. \\
&\quad \left. \left. - [\mathbf{D}_{B,A,k} \tilde{\mathbf{F}}_k]_{i,i} \left(\tilde{\lambda}_{A,B,kl}(\mathcal{A}) + \tilde{\lambda}_{kl}(\mathcal{A}) \tilde{\mathbf{F}}_k \tilde{\mathbf{F}}_l \tilde{\Xi}_{kl} \mathbf{\Lambda}_{A,B,kl} \right) \right] \mathbf{e}_i + [\mathbf{D}_{B,A,k} \mathbf{D}_{A,B,l} \tilde{\mathbf{F}}_k \tilde{\mathbf{F}}_l]_{i,i} [\tilde{\lambda}_{kl}(\mathcal{A}) \tilde{\Xi}_{kl}]_i \right\} + \mathcal{O}(N^{-\frac{1}{2}}) \\
&\stackrel{(a)}{=} \left(\tilde{\lambda}_{B,B,kl}(\mathcal{A}) + \tilde{\lambda}_{kl}(\mathcal{A}) \tilde{\mathbf{F}}_k \tilde{\mathbf{F}}_l \tilde{\Xi}_{kl} \mathbf{\Lambda}_{B,B,kl} - \tilde{\lambda}_{B,A,kl}(\mathcal{A}) \mathbf{D}_{A,B,l} \tilde{\mathbf{F}}_l - \tilde{\lambda}_{kl}(\mathcal{A}) \tilde{\mathbf{F}}_k \tilde{\mathbf{F}}_l \tilde{\Xi}_{kl} \mathbf{\Lambda}_{B,A,kl} \mathbf{D}_{A,B,l} \tilde{\mathbf{F}}_l \right. \\
&\quad \left. - \tilde{\lambda}_{A,B,kl}(\mathcal{A}) \mathbf{D}_{B,A,k} \tilde{\mathbf{F}}_k - \tilde{\lambda}_{kl}(\mathcal{A}) \tilde{\mathbf{F}}_k \tilde{\mathbf{F}}_l \tilde{\Xi}_{kl} \mathbf{\Lambda}_{A,B,kl} \mathbf{D}_{B,A,k} \tilde{\mathbf{F}}_k + \tilde{\lambda}_{kl}(\mathcal{A}) \tilde{\mathbf{F}}_k \tilde{\mathbf{F}}_l \tilde{\Xi}_{kl} \mathbf{D}_{B,A,k} \mathbf{D}_{A,B,l} \right) \mathbf{1}_M + \mathcal{O}(N^{-\frac{1}{2}}).
\end{aligned} \tag{86}$$

APPENDIX E PROOF OF COROLLARY 2

According to Corollary 1, we know that δ_k is the positive solution of the following equation

$$\delta_k(\rho_k) = \frac{1}{\rho_k(\tilde{\sigma}^2 + 1) + \frac{M+1}{N_k} \tilde{\sigma}^2 + \frac{M}{N_k} \frac{1}{1+\delta_k(\rho_k)}}. \tag{87}$$

By taking the derivative w.r.t. ρ_k , we have

$$\frac{\partial \delta_k}{\partial \rho_k} = -\frac{(\tilde{\sigma}^2 + 1) \delta_k^2}{V_k}, \tag{88}$$

where $V_k = 1 - \frac{M}{N_k} \frac{\delta_k^2}{(1+\delta_k)^2}$ and it can be proved that $V_k > 0$. Plugging this result into (28a) yields

$$\bar{\gamma}_K^{\text{foc}} = \sum_{k=1}^K \frac{\delta_k^2}{\delta_k + (\rho_k - \frac{\sigma^2}{N_k}) \frac{\partial \delta_k}{\partial \rho_k}} := \sum_{k=1}^K \bar{\gamma}_{K,k}^{\text{foc}}. \tag{89}$$

By taking the derivative, we obtain

$$\frac{\partial \bar{\gamma}_K^{\text{foc}}}{\partial \rho_k} = \frac{\partial \bar{\gamma}_{K,k}^{\text{foc}}}{\partial \rho_k} = \frac{[2(\frac{\partial \delta_k}{\partial \rho_k})^2 - \delta_k \frac{\partial^2 \delta_k}{\partial \rho_k^2}] (\rho_k - \frac{\sigma^2}{N_k}) \delta_k}{[\delta_k + (\rho_k - \frac{\sigma^2}{N_k}) \frac{\partial \delta_k}{\partial \rho_k}]^2}. \tag{90}$$

By taking the second-order derivative of δ_k , we have

$$2 \left(\frac{\partial \delta_k}{\partial \rho_k} \right)^2 - \delta_k \frac{\partial^2 \delta_k}{\partial \rho_k^2} = -\frac{2M(\tilde{\sigma}^2 + 1)^2 \delta_k^6}{N_k V_k^3 (1 + \delta_k)^3} < 0. \tag{91}$$

Hence, the optimal solution is given by $\rho_k^* = \frac{\sigma^2}{N_k} = \arg \max_{\rho_k > 0} \bar{\gamma}_{K,k}^{\text{foc}}$. Since ρ_k is independent with $\bar{\gamma}_{K,l}^{\text{foc}}$ for $l \neq k$, the optimal $\boldsymbol{\rho}_K$ is given by $\boldsymbol{\rho}_K^* = [\frac{\sigma^2}{N_1}, \dots, \frac{\sigma^2}{N_K}]^T$, which concludes (31). \square

APPENDIX F PROOF OF COROLLARY 3

Let $\rho_k = \frac{a}{c_k}$, $\forall k$ and define $A = a(\tilde{\sigma}^2 + 1) + \frac{M+1}{M} \tilde{\sigma}^2$ and $f(x) = Ax + \frac{x}{1+x}$. Then we consider the following equation

$$f(x) = c, \tag{92}$$

with $c \geq 0$. It can be proved that (92) has a unique positive solution $x = \delta(c)$ and we can observe that $\delta_k = \delta(c_k)$. Furthermore, we define

$$\tilde{\gamma}(c) = \frac{\delta(c)}{1 + B \frac{\delta(c)}{c - \frac{\delta^2(c)}{(1+\delta(c))^2}}}, \tag{93}$$

where $B = (\frac{\sigma^2}{M} - a)(\tilde{\sigma}^2 + 1)$. Then we can obtain $\bar{\gamma}_K^{\text{foc}}(\boldsymbol{\rho}_K, \mathbf{c}_K) = \sum_{k=1}^K \tilde{\gamma}(c_k)$. Taking the derivative of $f(\delta(c)) = c$ w.r.t. c yields

$$\begin{aligned}
\frac{\partial \delta}{\partial c} &= \frac{1}{A + \frac{1}{(1+\delta)^2}}, \quad \frac{\partial^2 \delta}{\partial c^2} = \frac{2(\frac{\partial \delta}{\partial c})^3}{(1+\delta)^3}, \\
\frac{\partial^3 \delta}{\partial c^3} &= \frac{6(\frac{\partial \delta}{\partial c})^4}{(1+\delta)^4} \left(\frac{\partial \delta}{\partial c} \frac{2}{(1+\delta)^2} - 1 \right),
\end{aligned} \tag{94}$$

where $\delta = \delta(c)$. Next we will prove (32). By taking the sum $\sum_{k=1}^K c_k = \sum_{k=1}^K f(\delta_k)$, we have

$$K\bar{c} = A \sum_{k=1}^K \delta_k + \sum_{k=1}^K \frac{\delta_k}{1 + \delta_k} \stackrel{(a)}{\geq} f\left(\sum_{k=1}^K \delta_k\right), \tag{95}$$

where step (a) follows from the inequality $\frac{x}{1+x} + \frac{y}{1+y} \geq \frac{x+y}{1+x+y}$ for $x, y \geq 0$. Since f is monotonically increasing, we have $\sum_{k=1}^K \delta_k \leq \delta(K\bar{c})$. Through basic transformation, we can obtain

$$\frac{\delta}{c - \frac{\delta^2}{(1+\delta)^2}} = \frac{1}{A + \frac{1}{(1+\delta)^2}} = \frac{\partial \delta}{\partial c}. \tag{96}$$

By (93) and (96), the following holds

$$\sum_{k=1}^K \tilde{\gamma}(c_k) = \sum_{k=1}^K \frac{\delta(c_k)}{1 + B \frac{\partial \delta(c_k)}{\partial c}} \stackrel{(a)}{\leq} \frac{\sum_{k=1}^K \delta(c_k)}{1 + B \frac{\partial \delta(K\bar{c})}{\partial c}} \leq \tilde{\gamma}(K\bar{c}), \tag{97}$$

where step (a) follows from $B \leq 0$ for $a \geq \frac{\sigma^2}{M}$ and $\frac{\partial^2 \delta}{\partial c^2} \geq 0$. Therefore, (32) holds.

Next, we assume that $\frac{\sigma^2}{M} \leq a \leq \frac{2\sigma^2}{M} + \frac{(M+1)\tilde{\sigma}^2}{M(\tilde{\sigma}^2+1)}$. We will first prove $\tilde{\gamma}(c)$ is convex. For that purpose, we take the second-order derivative of $\tilde{\gamma}$ w.r.t. c as

$$\begin{aligned}
\frac{\partial^2 \tilde{\gamma}}{\partial c^2} &= \frac{1}{(1 + B \frac{\partial \delta}{\partial c})^2} \left\{ - (B^2 \delta \frac{\partial \delta}{\partial c} + B \delta) \frac{\partial^3 \delta}{\partial c^3} \right. \\
&\quad \left. + 2B^2 \delta (\frac{\partial^2 \delta}{\partial c^2})^2 - (B^2 (\frac{\partial \delta}{\partial c})^2 - 1) \frac{\partial^2 \delta}{\partial c^2} \right\}.
\end{aligned} \tag{98}$$

Thus, to prove $\frac{\partial^2 \tilde{\gamma}}{\partial c^2} \geq 0$, it is sufficient to show that

$$(-2pq^2 + 3(1-2p)q - 1)\delta \leq 1 - q^2, \tag{99}$$

where $p = A \frac{\partial \delta}{\partial c}$ and $q = B \frac{\partial \delta}{\partial c}$. For $\frac{\sigma^2}{M} \leq a \leq \frac{2\sigma^2}{M} + \frac{(M+1)\tilde{\sigma}^2}{M(\tilde{\sigma}^2+1)}$, it holds true that $-\frac{1}{2} \leq \frac{B}{A} = \frac{q}{p} \leq 0$. From (94), it can be observed that $0 \leq p < 1$. Hence, we can obtain

$$\sup_{p \in [0,1], q \in [-\frac{1}{2}, 0]} -2pq^2 + 3(1-2p)q - 1 = 0, \tag{100}$$

to conclude (99). According to Jensen's inequality, we have

$$\sum_{k=1}^K \tilde{\gamma}(c_k) \geq K \tilde{\gamma}(\bar{c}) = \bar{\gamma}_K^{\text{foc}}(\boldsymbol{\rho}_K, \mathbf{c}_{K,m}), \tag{101}$$

which completes the proof of Corollary 3. \square

APPENDIX G PROOF OF COROLLARY 4

In this proof, we will reuse the notations in Appendix F. Moreover, we define $c_{\text{sum}} = \frac{N}{M}$. By (96), the SINR is given by

$$\bar{\gamma}_K^{\text{foc}}(\boldsymbol{\rho}_K, \mathbf{c}_{K,m}) = \frac{K \bar{\delta}_K}{1 + \frac{B}{A + \frac{1}{(1+\bar{\delta}_K)^2}}}, \tag{102}$$

where $\bar{\delta}_K$ is the unique positive solution of the following quadratic equation

$$f(\bar{\delta}_K) = \frac{c_{\text{sum}}}{K}. \quad (103)$$

Since $f(x)$ is monotonically increasing w.r.t. x , $\bar{\delta}_K$ monotonically decreases w.r.t. K . Additionally, (103) implies

$$K\bar{\delta}_K = \frac{c_{\text{sum}}}{A + \frac{1}{1+\bar{\delta}_K}}, \quad (104)$$

which further indicates that $K\bar{\delta}_K$ is also monotonically decreasing. Since $a \geq \frac{\sigma^2}{M}$, we have $B \leq 0$ and

$$\begin{aligned} \bar{\gamma}_K^{\text{foc}}(\rho_K, \mathbf{c}_{K,m}) &\geq \frac{(K+1)\bar{\delta}_{K+1}}{1 + \frac{B}{A + \frac{1}{(1+\bar{\delta}_K)^2}}} \\ &\geq \frac{(K+1)\bar{\delta}_{K+1}}{1 + \frac{B}{A + \frac{1}{(1+\bar{\delta}_{K+1})^2}}} = \bar{\gamma}_{K+1}^{\text{foc}}(\rho_{K+1}, \mathbf{c}_{K+1,m}), \end{aligned} \quad (105)$$

which conclude (34). \square

REFERENCES

- [1] L. Lu, G. Y. Li, A. L. Swindlehurst, A. Ashikhmin, and R. Zhang, "An overview of massive MIMO: Benefits and challenges," *IEEE J. Select. Topics Signal Process.*, vol. 8, no. 5, pp. 742–758, Apr. 2014.
- [2] C. Jeon, K. Li, J. R. Cavallaro, and C. Studer, "Decentralized equalization with feedforward architectures for massive MU-MIMO," *IEEE Trans. Signal Process.*, vol. 67, no. 17, pp. 4418–4432, Sep. 2019.
- [3] L. Van der Perre, L. Liu, and E. G. Larsson, "Efficient DSP and circuit architectures for massive MIMO: State of the art and future directions," *IEEE Trans. Signal Process.*, vol. 66, no. 18, pp. 4717–4736, Sep. 2018.
- [4] K. Li, R. R. Sharan, Y. Chen, T. Goldstein, J. R. Cavallaro, and C. Studer, "Decentralized baseband processing for massive MU-MIMO systems," *IEEE Trans. Emerg. Sel. Topics Circuits Syst.*, vol. 7, no. 4, pp. 491–507, Dec. 2017.
- [5] Y. Xu, E. G. Larsson, E. A. Jorswieck, X. Li, S. Jin, and T.-H. Chang, "Distributed signal processing for extremely large-scale antenna array systems: State-of-the-art and future directions," *arXiv preprint arXiv:2407.16121*, 2024.
- [6] K. Li, Y. Chen, R. Sharan, T. Goldstein, J. R. Cavallaro, and C. Studer, "Decentralized data detection for massive MU-MIMO on a Xeon Phi cluster," in *Proc. Conf. Rec. 50th Asilomar Conf. Signals, Syst. Comput. (ASILOMAR)*, 2016, pp. 468–472.
- [7] J. Rodríguez Sánchez, F. Rusek, O. Edfors, M. Sarajlić, and L. Liu, "Decentralized massive MIMO processing exploring daisy-chain architecture and recursive algorithms," *IEEE Trans. Signal Process.*, vol. 68, pp. 687–700, 2020.
- [8] K. Li, J. McNaney, C. Tarver, O. Castañeda, C. Jeon, J. R. Cavallaro, and C. Studer, "Design trade-offs for decentralized baseband processing in massive MU-MIMO systems," in *Proc. Conf. Rec. 53rd Asilomar Conf. Signals, Syst. Comput. (ASILOMAR)*, 2019, pp. 906–912.
- [9] K. Li, C. Jeon, J. R. Cavallaro, and C. Studer, "Decentralized equalization for massive MU-MIMO on FPGA," in *Proc. Conf. Rec. 51st Asilomar Conf. Signals, Syst. Comput. (ASILOMAR)*, 2017, pp. 1532–1536.
- [10] F. Rusek, D. Persson, B. K. Lau, E. G. Larsson, T. L. Marzetta, O. Edfors, and F. Tufvesson, "Scaling up MIMO: Opportunities and challenges with very large arrays," *IEEE Signal Process. Mag.*, vol. 30, no. 1, pp. 40–60, Jan. 2013.
- [11] H. Q. Ngo, A. Ashikhmin, H. Yang, E. G. Larsson, and T. L. Marzetta, "Cell-free massive MIMO versus small cells," *IEEE Trans. Wireless Commun.*, vol. 16, no. 3, pp. 1834–1850, Mar. 2017.
- [12] E. Björnson and L. Sanguinetti, "Making cell-free massive MIMO competitive with MMSE processing and centralized implementation," *IEEE Trans. Wireless Commun.*, vol. 19, no. 1, pp. 77–90, Jan. 2020.
- [13] J. Zhang, C.-K. Wen, S. Jin, X. Gao, and K.-K. Wong, "Large system analysis of cooperative multi-cell downlink transmission via regularized channel inversion with imperfect CSIT," *IEEE Trans. Wireless Commun.*, vol. 12, no. 10, Oct. 2013.
- [14] Z. Wei, D. Xu, S. Li, S. Song, D. W. K. Ng, and G. Caire, "Resource allocation design for next-generation multiple access: A tutorial overview," *arXiv preprint arXiv:2407.02877*, 2024.
- [15] A. Kammoun, M. Kharouf, W. Hachem, and J. Najim, "A central limit theorem for the SINR at the LMMSE estimator output for large-dimensional signals," *IEEE Trans. Inf. Theory*, vol. 55, no. 11, pp. 5048–5063, Nov. 2009.
- [16] A. Kammoun *et al.*, "BER and outage probability approximations for LMMSE detectors on correlated MIMO channels," *IEEE Trans. Inf. Theory*, vol. 55, no. 10, pp. 4386–4397, Oct. 2009.
- [17] X. Zhang, S. Song, and Y. C. Eldar, "Secrecy analysis for MISO broadcast systems with regularized zero-forcing precoding," *arXiv preprint arXiv:2301.11515*, 2023.
- [18] X. Zhao, M. Li, Y. Liu, T.-H. Chang, and Q. Shi, "Communication-efficient decentralized linear precoding for massive MU-MIMO systems," *IEEE Trans. Signal Process.*, vol. 71, pp. 4045–4059, 2023.
- [19] X. Zhao, M. Li, B. Wang, E. Song, T.-H. Chang, and Q. Shi, "Decentralized equalization for massive MIMO systems with colored noise samples," *arXiv preprint arXiv:2305.12805*, 2023.
- [20] J. Hoydis, S. ten Brink, and M. Debbah, "Massive MIMO in the UL/DL of cellular networks: How many antennas do we need?" *IEEE J. Select. Areas Commun.*, vol. 31, no. 2, pp. 160–171, Feb. 2013.
- [21] S. Wagner, R. Couillet, M. Debbah, and D. T. M. Slock, "Large system analysis of linear precoding in correlated MISO broadcast channels under limited feedback," *IEEE Trans. Inf. Theory*, vol. 58, no. 7, pp. 4509–4537, Jul. 2012.
- [22] J. Hoydis, M. Kobayashi, and M. Debbah, "Asymptotic performance of linear receivers in network MIMO," in *Proc. Conf. Rec. 44th Asilomar Conf. Signals, Syst. Comput. (ASILOMAR)*, 2010, pp. 942–948.
- [23] Y. Xu, B. Wang, E. Song, Q. Shi, and T.-H. Chang, "Low-complexity channel estimation for massive MIMO systems with decentralized baseband processing," *IEEE Trans. Signal Process.*, vol. 71, pp. 2728–2743, Jul. 2023.
- [24] E. Björnson, J. Hoydis, and L. Sanguinetti, *Massive MIMO Networks: Spectral, Energy, and Hardware efficiency*. London, U.K.: Now Found. Trends, 2017.
- [25] B. Picinbono, "Second-order complex random vectors and normal distributions," *IEEE Trans. Signal Process.*, vol. 44, no. 10, pp. 2637–2640, Oct. 1996.
- [26] A. Abrardo, G. Fodor, M. Moretti, and M. Telek, "MMSE receiver design and SINR calculation in MU-MIMO systems with imperfect CSI," *IEEE Wireless Commun. Lett.*, vol. 8, no. 1, pp. 269–272, Feb. 2019.
- [27] B. Hassibi and B. Hochwald, "How much training is needed in multiple-antenna wireless links?" *IEEE Trans. Inf. Theory*, vol. 49, no. 4, pp. 951–963, Apr. 2003.
- [28] D. Guo, S. Shamai, and S. Verdú, "Mutual information and minimum mean-square error in Gaussian channels," *IEEE Trans. Inf. Theory*, vol. 51, no. 4, pp. 1261–1282, Apr. 2005.
- [29] A. W. Marshall, I. Olkin, and B. C. Arnold, *Inequalities: Theory of Majorization and its Applications*. New York, NY, USA: Academic Press, 1979.
- [30] J. Zhang, C.-K. Wen, S. Jin, X. Gao, and K.-K. Wong, "On capacity of large-scale MIMO multiple access channels with distributed sets of correlated antennas," *IEEE J. Select. Areas Commun.*, vol. 31, no. 2, pp. 133–148, Jan. 2013.
- [31] X. Zhang and S. Song, "Secrecy analysis for IRS-aided wiretap MIMO communications: Fundamental limits and system design," *IEEE Trans. Inf. Theory*, pp. 1–1, Nov. 2023.
- [32] A. Kammoun and M.-S. Alouini, "No eigenvalues outside the limiting support of generally correlated Gaussian matrices," *IEEE Trans. Inf. Theory*, vol. 62, no. 7, pp. 4312–4326, Jul. 2016.
- [33] A. W. Van der Vaart, *Asymptotic Statistics*. Cambridge, U.K.: Cambridge University Press, 1998.
- [34] L. A. Pastur and M. Shcherbina, *Eigenvalue Distribution of Large Random Matrices*. Providence, RI, USA: American Mathematical Society, 2011.
- [35] W. Hachem, O. Khorunzhiy, P. Loubaton, J. Najim, and L. Pastur, "A new approach for mutual information analysis of large dimensional multi-antenna channels," *IEEE Trans. Inf. Theory*, vol. 54, no. 9, pp. 3987–4004, Sep. 2008.
- [36] X. Zhang and S. Song, "Asymptotic mutual information analysis for double-scattering MIMO channels: A new approach by Gaussian tools," *IEEE Trans. Inf. Theory*, vol. 69, no. 9, pp. 5497–5527, Sep. 2023.
- [37] Z. Zhuang, X. Zhang, D. Xu, and S. Song, "Fundamental limits of two-hop MIMO channels: An asymptotic approach," *arXiv preprint arXiv:2402.03772*, 2024.
- [38] W. Hachem, P. Loubaton, and J. Najim, "A CLT for information-theoretic statistics of Gram random matrices with a given variance profile," *Ann. Appl. Probabil.*, vol. 18, no. 6, pp. 2071 – 2130, Dec. 2008.